

Alma Mater Studiorum Università di Bologna
Archivio istituzionale della ricerca

Finite-time continuous extended state observers: design and experimental validation on electro-hydraulic systems☆

This is the final peer-reviewed author's accepted manuscript (postprint) of the following publication:

Published Version:

Razmjooei H., Palli G., Abdi E., Strano S., Terzo M. (2022). Finite-time continuous extended state observers: design and experimental validation on electro-hydraulic systems☆. MECHATRONICS, 85, 1-17 [10.1016/j.mechatronics.2022.102812].

Availability:

This version is available at: <https://hdl.handle.net/11585/891150> since: 2022-07-22

Published:

DOI: <http://doi.org/10.1016/j.mechatronics.2022.102812>

Terms of use:

Some rights reserved. The terms and conditions for the reuse of this version of the manuscript are specified in the publishing policy. For all terms of use and more information see the publisher's website.

This item was downloaded from IRIS Università di Bologna (<https://cris.unibo.it/>).
When citing, please refer to the published version.

(Article begins on next page)

This is the final peer-reviewed accepted manuscript of:

Hamid Razmjooei, Gianluca Palli, Elahe Abdi, Salvatore Strano, Mario Terzo, Finite-time continuous extended state observers: design and experimental validation on electro-hydraulic systems☆, Mechatronics, Volume 85, 2022, 102812, ISSN 0957-4158.

The final published version is available online at:

<https://doi.org/10.1016/j.mechatronics.2022.102812>

Terms of use:

Some rights reserved. The terms and conditions for the reuse of this version of the manuscript are specified in the publishing policy. For all terms of use and more information see the publisher's website.

This item was downloaded from IRIS Università di Bologna (<https://cris.unibo.it/>)

When citing, please refer to the published version.

Finite-Time Continuous Extended State Observers: Design and Experimental Validation on Electro-Hydraulic Systems

Hamid Razmjooei^{a*}, Gianluca Palli^a, Elahe Abdi^b, Salvatore Strano^c, and Mario Terzo^c

^a Department of Electrical Energy and Information Engineering, University of Bologna, Bologna, Italy
(Emails: hamid.razmjooei@unibo.it, gianluca.palli@unibo.it)

^b Department of Mechanical and Aerospace Engineering, Monash University, Melbourne, Australia
(Email: elahe.abdi@monash.edu)

^c Department of Industrial Engineering, University of Naples Federico II, Naples, Italy (Emails: salvatore.strano@unina.it, mario.terzo@unina.it)

* Corresponding author: **Hamid Razmjooei**

Abstract:

In this paper, a time-varying chattering-free observer for electro-hydraulic actuators able to provide finite-time estimations of the full state variables as well as uncertainties is presented. The key idea is to employ a positive-increasing function associated with the observer objectives to improve the convergence time performance. First, the model of an electro-hydraulic actuator as a case study for the proposed observer is presented. Then, an extended state observer is introduced, and the time-varying gains are provided to ensure that without neither any knowledge about the upper bounds of the uncertainties nor its derivative, the observation error dynamics is convergent to a neighborhood of zero in a finite time. Comparative simulations are presented to analyze the effectiveness of the proposed observers. Then, further simulations are performed in the presence of measurement noise. It is concluded that the proposed scheme can compete with other leading strategies, making it a qualified alternative approach in the observer design with noteworthy potential. Finally, the effectiveness of the proposed approach in real-life conditions is demonstrated through experimental studies.

Keywords: *Electro hydraulic actuator systems, Extended-state nonlinear observers, Time-varying transformation, Uncertainties.*

1. Introduction

Electro-Hydraulic Actuators (EHAs) have been widely used in robots and aircrafts due to their advantages in terms of reliability, power density and maximum force. However, EHAs are affected by several uncertainties and strong non-linearities, including unmodeled dynamics, disturbances, and considerable friction, limiting their broad applicability [1, 2]. In the presence of these non-idealities, exact modeling is not feasible. A simple solution in dealing with the intrinsic problems and limitations of EHAs is to equip the system with various sensors. However, measuring the full system states is very challenging and often impossible in practice, due to issues such as cost, complexity, space limitations, and

measurement noise. Therefore, estimating the state variables is essential in achieving an acceptable dynamic performance in EHAs. In practice, an alternative approach is to sensorize the main output of the system and design an observation algorithm to process the incomplete information collected by the sensors and construct a reliable estimation of all state variables [3]. Thus, the observer is an authoritative option to provide an estimate for state variables and subsequently reduce the number of sensors [4]. To estimate either unmeasured states or uncertainties, several approaches have been reported in the literature. On the other hand, to estimate the unmeasured states and uncertainties simultaneously, the extended state observers (ESO) have

been introduced [5]. In addition, in the presence of unknown terms such as uncertainties, external disturbances, and friction, exact estimation of state variables is impossible, and instead, the ultimate boundedness concept must be considered [6].

Many observation approaches provide an asymptotic or exponential convergence implying the convergence of the observation errors to a neighborhood of zero over an infinite time interval. However, in many applications of EHA, such as medical robotics and aircraft actuators, high steady-state precision performance as well as finite-time convergence is of paramount importance to meet the precision and safety requirements [7]. Within the finite-time observer context, several strategies have been presented by academic and industrial researchers. The Sliding Mode Observer (SMO) is one of the main methods with widespread applications. Two benchmark studies on SMOs are reported in [8, 9]. This approach has been further developed in recent years and several applications can be found in [10-13], where the performance of the observers is investigated through simulation, considering different sets of measurement noises, parametric uncertainties, and model nonlinearities. For instance, in [13] this strategy is developed for nonlinear systems with unknown inputs. In spite of the successful deployment of SMO, its standard version is affected by some restrictions, leading to the potentially destructive chattering phenomenon in their convergence to a small neighborhood of zero [14]. To mitigate this drawback, alternative approaches have been developed, such as the High-order Sliding Mode Observer (HSMO) to reduce the chattering and the Terminal Sliding Mode Observer (TSMO) with finite-time convergence properties [15, 16]. For instance, in [15] the evaluation

of different robust observation techniques including SMO and HSMO compared with the Extended Kalman filter method is presented. The HSMO technique is well-developed with numerous applications [17-20]. However, successful results in [15-20] were inspired by the high-order sliding-mode differentiator [21] frequently associated with structural limitations of higher-order uncanonical systems.

In spite of the extensive and successful development of the SMO method, one problem remains: the convergence time grows unboundedly if the initial conditions tend far from the equilibrium point. Thus, it is desirable for an observer to guarantee that the convergence is achieved in a fixed-time interval regardless of initial conditions. Fixed-time observers using the concept of bi-limit homogeneity were first introduced in [22] and then were studied in [23-25]. The fixed-time approach is more powerful than the finite-time approach as it guarantees the boundedness of the convergence time independent of initial conditions. However, in addition to structural limitations, the gains of these observers are not easily computable. Moreover, defining a proper Lyapunov function to prove the observer stability is not straightforward for high-order systems. Hence, within this context, the state estimation in a finite time remains a challenge, where a straightforward observer design to estimate the full state of systems, as well as the uncertainties, in a finite time is still an open problem. In recent years, high-gain and time-varying observers have been well-investigated [26-30]. For instance, a time-varying observer with an exponential convergence is presented in [26]. Additionally, a time-varying observer is presented in [29] with the following shortcomings: (1) Valid response only in a finite time interval, while in many applications it is important

to have a valid response for a longer duration; (2) Unconsidered internal dynamics, while internal dynamics should be explicitly considered in the proof as it can act as an uncertainty in the values of the state variables; (3) Required prior knowledge of the uncertainties, while it is not often possible to measure them in practice. To overcome these restrictions, a time-varying observer, known as finite-time ESO, is presented in [30]. This observer is able to estimate the full state of systems as well as the uncertainties in finite time. Compared with the existing strategies, its main advantages are the straightforward design and the robustness against uncertainties and internal dynamics. However, its main limitation is the singularity problem, where the proposed time-varying transformation grows unboundedly when time tends to infinity. In addition, even if this observer is a valid scheme to estimate uncertainties, it is only applicable in single-input single-output canonical systems. With this background, we conclude that the two approaches of HSMO in [15, 17], and high-gain extended state observer (HGESO) in [27] have better performance for EHA systems under parametric uncertainties and model nonlinearities, where dead-zone functions have been considered to describe realistic control valves. The HSMO was analyzed compared with SMO and its high efficiency in the estimation of the uncertainties was shown [15, 17]. In addition, HGESO was analyzed compared with conventional observers, and it was shown that it estimated the full state and total disturbance quite well [27, 28]. Consequently, despite several studies and with the exception of these two leading strategies, the finite-time ESO subject still boasts potential for further improvement.

Motivated by the above considerations, in this paper a time-varying observer for EHAs is designed,

in which, without neither any knowledge about the upper bounds of the uncertainties nor its derivative, the estimation of the full state variables, as well as uncertainties, is achieved. The key idea is to employ a positive-increasing function associated with the observer objectives to improve the convergence time performance. To this end, the EHA model based on the proper behavior for each state variable is divided into three parts. Then, the extended state observers are designed for each part, independently. To design the ESOs, auxiliary variables are introduced based on uncertainties. By defining a time-varying transformation, the time-varying gains of each observer are designed by using the asymptotic stability methods, so that the observation error variables tend to the neighborhood of zero without any chattering and remain uniformly bounded in a finite time. Finally, to highlight the efficiency of the proposed framework, several comparative simulations are reported between the proposed finite-time ESO, and the two leading strategies of HSMO [15] and HGESO [27]. Moreover, the performance of the proposed framework in presence of measurement noise is validated in simulations. Finally, its effectiveness in the presence of external load is demonstrated in an experimental study. Compared with the existing literature, the main contributions of this paper are: (1) A continuous and chattering-free ESO is designed, using which, without neither any knowledge about the upper bound of uncertainties nor its derivative, it is possible to estimate the full state of the nonlinear system as well as the uncertainties, achieving convergence of the observation error to a neighborhood of zero. (2) A time-varying conversion is introduced such that the state estimation is guaranteed with finite-time boundedness properties by using the asymptotic stability methods in a straightforward manner. (3) Time-

varying gains are computed based on straightforward algebraic equations, and their values are valid in long time intervals.

The remainder of the paper is structured as follows. In Section 2, a fifth-order model of the EHA is illustrated and relevant definitions are presented. In Section 3, the time-varying ESOs are designed. To characterize the finite-time property, a novel change of coordinates is adopted, and subsequently, time-varying gains are designed, so that convergence of the observation errors to a neighborhood of zero in a finite time is guaranteed. In Sections 4 and 5, simulation and experimental results demonstrate the effectiveness of the designed finite-time ESO for the fifth-order uncertain EHAs. Finally, conclusions and the future plans are presented in Section 6.

2. Preliminaries and System Dynamics

EHAs mostly consist of a double-rod hydraulic cylinder and a proportional valve [15]. The schematic diagram of a generic EHA is reported in Fig. 1.

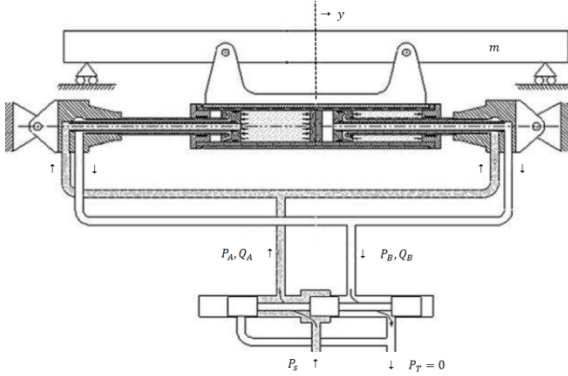


Fig. 1. Graphical representation of the hydraulic actuation system [15].

To design the observer, the mathematical model (1) of EHA is considered [15]; where for convenience the time variable t may be omitted.

$$\begin{aligned}\ddot{y} &= -\frac{b}{m}\dot{y} - \frac{F_f(\dot{y})}{m} + \frac{A_P P_L}{m} \\ \dot{P}_L &= -\frac{2\rho A_P}{V_0}\dot{y} + \frac{2\rho\Psi(v_e)\sqrt{P_s - |P_L|}}{V_0} \\ \ddot{v}_e &= -\omega_{nv}^2 v_e - 2\epsilon_v \omega_{nv} \dot{v}_e \\ &\quad + \omega_{nv}^2 (k_e u + v_{e0})\end{aligned}\quad (1)$$

where y , P_L and v_e are the piston position, the load pressure, and the spool valve displacement signal, respectively.

According to Fig. 1, $P_L = P_A - P_B$, where P_A and P_B are the pressures inside the two-cylinder chambers. Besides, Q_A and Q_B are the flows inside the two-cylinder chambers. b is the viscous friction coefficient, m is the mass of the load, $F_f(\dot{y})$ is the friction force, A_P is the piston area, ρ is the effective Bulk modulus, V_0 is the volume of each chamber for the piston centered position, $\Psi(v_e)$ is a gain that depends on the geometry of the adopted proportional valve, P_s and P_T are the supply and the tank pressures respectively, ω_{nv} and ϵ_v are the natural frequency and the damping ratio of the valve respectively, k_e is the input gain, u is the valve command, and v_{e0} is the spool position bias [15].

Assumption 1. In this paper, only the vector $h(t, x(t)) = [y \ P_L \ v_e]^T$ as the output of the system is measurable and available online.

Assumption 2 [15]. In this paper, it is assumed that the viscous friction coefficient, the valve natural frequency, and the damping coefficient have already been identified experimentally. In general, these coefficients are not easy to measure and obtain, and are often treated as uncertainties.

Now based on (1), $x(t) = [y(t) \ \dot{y}(t) \ P_L(t) \ v_e(t) \ \dot{v}_e(t)]^T$ is considered as the state vector, $u(t) = u$ and $z(t) = h(t, x)$ are presented as the input and output, respectively; thus, the hydraulic actuation system (1) can be rewritten in the following state space form.

$$\begin{aligned}\dot{x}(t) &= f(t, x) + gu(t) + \bar{\varphi}(t, x) \\ z(t) &= h(t, x)\end{aligned}\quad (2)$$

where

$$f(t, x) = \begin{bmatrix} \dot{y} \\ -\frac{b}{m}\dot{y} + \frac{A_P P_L}{m} \\ \frac{2\rho k_q v_e \sqrt{P_s - |P_L|}}{V_0} \\ \dot{v}_e \\ -\omega_{nv}^2 v_e - 2\epsilon_v \omega_{nv} \dot{v}_e \end{bmatrix}$$

$$g = \begin{bmatrix} 0 \\ 0 \\ 0 \\ 0 \\ \omega_{nv}^2 k_e \end{bmatrix}$$

$$\bar{\varphi}(t, x) = \begin{bmatrix} 0 \\ -\frac{F_f(\dot{y})}{m} + \eta_y(t) \\ \tilde{\varphi} + \eta_{P_L}(t) \\ 0 \\ \omega_{nv}^2 v_{e0} + \eta_{v_e}(t) \end{bmatrix}$$

wherein

$\tilde{\varphi} = \frac{-2\rho A_P \dot{y}}{V_0} + \frac{2\rho(\Psi(v_e) - k_q v_e) \sqrt{P_s - |P_L|}}{V_0}$, k_q is the nominal valve constant, and $\eta = [\eta_y(t) \ \eta_{P_L}(t) \ \eta_{v_e}(t)]^T$ includes unmodeled loads, dynamics, and parameter uncertainties [17]. The first equation in (1) represents the piston rod dynamics, including any other model part related to it; the second one describes the load pressure dynamics, and the third one follows the proportional valve dynamics [15]. As mentioned in the introduction, in this paper the EHA dynamic based on the proper behavior for each state variable is divided into three subsystems, and subsequently, three finite-time ESOs are designed, separately. Hence, the state vector $x(t)$ may be separated as $x_1(t) = [y(t), \dot{y}(t)]^T$, $x_2(t) = P_L(t)$, and $x_3(t) = [v_e(t), \dot{v}_e(t)]^T$. Subsequently, the state-space (2) can be rewritten as,

$$\dot{x}_1(t) = f_1(t, x) + g_1 u(t) + \bar{\varphi}_1(t, x) \quad (3)$$

$$\dot{x}_2(t) = f_2(t, x) + g_2 u(t) + \bar{\varphi}_2(t, x) \quad (4)$$

$$\dot{x}_3(t) = f_3(t, x) + g_3 u(t) + \bar{\varphi}_3(t, x) \quad (5)$$

where the certain dynamics are defined

$$\text{as } f_1(t, x) = \left[\dot{y}, -\frac{b}{m}\dot{y} + \frac{A_P P_L}{m} \right]^T,$$

$$f_2(t, x) = \frac{2\rho k_q v_e \sqrt{P_s - |P_L|}}{V_0}, \text{ and } f_3(t, x) =$$

$$[\dot{v}_e, -\omega_{nv}^2 v_e - 2\epsilon_v \omega_{nv} \dot{v}_e]^T. \text{ Also}$$

$$g_1 = [0, 0]^T, \quad g_2 = 0, \quad \text{and} \quad g_3 = [0, \omega_{nv}^2 k_e]^T. \text{ Finally, uncertainties are}$$

$$\text{presented as } \bar{\varphi}_1(t, x) = \left[0, -\frac{F_f(\dot{y})}{m} + \right.$$

$$\left. \eta_y(t) \right]^T, \quad \bar{\varphi}_2(t, x) = -\frac{2\rho A_P}{V_0} \dot{y} +$$

$$\frac{2\rho(\Psi(v_e) - k_q v_e) \sqrt{P_s - |P_L|}}{V_0} + \eta_{P_L}(t), \quad \text{and}$$

$$\bar{\varphi}_3(t, x) = [0, \omega_{nv}^2 v_{e0} + \eta_{v_e}(t)]^T. \text{ It is}$$

noted that due to the uncertainties $\bar{\varphi}_i(t, x)$, the exact

convergence to zero in a finite time is impossible, and instead, the ultimate

boundedness concept is considered. In this paper, the following fundamental

definitions are used:

Definition 1 ([31]). The system $\dot{z} = \chi(t, z, \delta)$ is said to be bounded in a finite time T with respect to δ where $\|\delta\| \leq \sigma$, if for an assumed positive-definite (PD) matrix function Z , a PD matrix Z_0 , and any positive constants a , b , and σ , where $0 \leq a \leq b$, one has $z^T Z z < b$ in $t \in [0, T]$ whenever $z_0^T Z_0 z_0 \leq a$.

Definition 2 ([4, 31]). The system $\dot{z} = \chi(t, z, \delta)$ is said to be finite-time input-to-state stable (FT-ISS) in a finite time T with respect to δ where $\|\delta\| \leq \sigma$, if the inequality (6) for functions α and β is guaranteed for any $t \geq t_0 + T$:

$$\|z\| \leq \alpha(\|z_0\|, \bar{\vartheta}) + \beta(\|\delta\|) \quad (6)$$

where α and β are KL -class and K -class functions, respectively. Also, $\bar{\vartheta}$ is a time-varying function tending to infinity as $t \rightarrow t_0 + T$. It is worth noting that, in the absence of the disturbance δ , an FT-ISS

system will be finite-time stable (FTS) [18].

Remark 1. Consider the change of coordinates $\Sigma_1 \rightarrow \Sigma_2$ in form of $\Sigma_2 = C\Sigma_1$, where C is defined as a positive incremental function, and diverging asymptotically to infinity as $t \rightarrow t_0 + T$. Then, if the variable Σ_2 remains stable, which does not tend to infinity, the boundedness of the first coordinate Σ_1 as $t \rightarrow t_0 + T$ is guaranteed.

Remark 2. According to Assumption 1, although, the output vector $[y \ P_L \ v_e]^T$ is measurable and available online, however, measuring or computing the time derivative of y , P_L , and v_e (i.e. \dot{y} , \dot{P}_L , and \dot{v}_e) appear as a potential challenge to analysis of the system. To mitigate this challenge and to reduce the number of sensors, an alternative approach is measuring the outputs y , P_L , and v_e with usual sensors and using the observers to construct a reliable estimation of \dot{y} , \dot{P}_L , and \dot{v}_e . Besides, since the uncertainties such as the external force such as the friction force, external disturbance, the dead-zone effects, and spool bias have appeared in the dynamics of \dot{y} , \dot{P}_L , and \dot{v}_e , respectively, therefore to simultaneously estimate the unmeasured states (the derivatives of output variables) and uncertainties, finite-time ESOs (10)-(12) will be designed in the next section.

3. Finite-Time ESO Design

In this Section, finite-time ESOs are designed for the subsystems (3)-(5), so that the estimations of state variables track real states in a finite time. The uncertainties $\varphi_1(t, x) = -\frac{F_f(y)}{m} + \eta_y(t)$, $\varphi_2(t, x) = \bar{\varphi}_2(t, x)$, and $\varphi_3(t, x) = \omega_{nv}^2 v_{e0} + \eta_{v_e}(t)$ are entered into the state vectors as auxiliary variables [7]; where the state vectors are updated as follow:

$$\begin{aligned} x_{1a}(t) &= [y(t), \dot{y}(t), \varphi_1(t, x)]^T \\ x_{2a}(t) &= [P_L(t), \varphi_2(t, x)]^T \end{aligned}$$

$$x_{3a}(t) = [v_e(t), \dot{v}_e(t), \varphi_3(t, x)]^T$$

then, the augmented subsystems (3)-(5) are achieved as,

$$\dot{x}_{1a}(t) = f_{1a}(t, x) + g_{1a}u(t) + \bar{\varphi}_{1a}(t, x) + B_1\dot{\varphi}_1(t, x) \quad (7)$$

$$\dot{x}_{2a}(t) = f_{2a}(t, x) + g_{2a}u(t) + \bar{\varphi}_{2a}(t, x) + B_2\dot{\varphi}_2(t, x) \quad (8)$$

$$\dot{x}_{3a}(t) = f_{3a}(t, x) + g_{3a}u(t) + \bar{\varphi}_{3a}(t, x) + B_3\dot{\varphi}_3(t, x) \quad (9)$$

where for $i = 1, 2$ and 3 , the vector B_i is defined as $B_i = [0_{n_i-1}, 1]^T$, in which $n_1 = n_3 = 3$ and $n_2 = 2$. Also, $0_{n_i} \in R^{n_i}$ are zero vectors. Besides, $f_{1a}(t, x) = [f_1(t, x)^T, 0]^T$, $f_{2a}(t, x) = [f_2(t, x), 0]^T$, $f_{3a}(t, x) = [f_3(t, x)^T, 0]^T$, $g_{1a} = [g_1^T, 0]^T$, $g_{2a} = [0, 0]^T$, and $g_{3a} = [g_3^T, 0]^T$. Moreover, $\bar{\varphi}_{1a}(t, x) = [\bar{\varphi}_1(t, x)^T, 0]^T$, $\bar{\varphi}_{2a}(t, x) = [\bar{\varphi}_2(t, x), 0]^T$, and $\bar{\varphi}_{3a}(t, x) = [\bar{\varphi}_3(t, x)^T, 0]^T$.

Assumption 3. In this paper, it is assumed $\dot{\varphi}_1(t, x)$, $\dot{\varphi}_2(t, x)$, and $\dot{\varphi}_3(t, x)$ are bounded as $|\dot{\varphi}_1(t, x)| \leq \sigma_1$, $|\dot{\varphi}_2(t, x)| \leq \sigma_2$, and $|\dot{\varphi}_3(t, x)| \leq \sigma_3$; where σ_1 , σ_2 , and σ_3 are non-negative constants as upper bounds of the amplitude of functions $\dot{\varphi}_1(t, x)$, $\dot{\varphi}_2(t, x)$, and $\dot{\varphi}_3(t, x)$, respectively.

Note that the positive real numbers σ_1 , σ_2 , and σ_3 may be unknown and they should just exist. The boundedness of these terms will be validated by the Simulation results; where these conditions are connected to the existence and uniqueness of solutions of systems (7)-(9) [32].

Since the sum of the relative degrees of the subsystems is equal to the order of the system ($n_1 + n_2 + n_3 = 5$), therefore observability is guaranteed. Now, we are in a position to design finite-time ESOs for the augmented subsystems (7)-(9). To simultaneously estimate the unmeasured states and the uncertainties, the following finite-time ESOs are proposed:

$$\hat{x}_{1a}(t) = f_{1a}(t, \hat{x}) + g_{1a}u(t) + K_1(t)(y - \hat{y}) \quad (10)$$

$$\hat{x}_{2a}(t) = f_{2a}(t, \hat{x}) + g_{2a}u(t) + K_2(t)(P_L - \hat{P}_L) \quad (11)$$

$$\hat{x}_{3a}(t) = f_{3a}(t, \hat{x}) + g_{3a}u(t) + K_3(t)(v_e - \hat{v}_e) \quad (12)$$

as the finite-time ESOs for subsystems 1, 2, and 3, respectively. Also, $K_1(t) = \text{diag}(k_{11}, k_{21}, k_{31})$, $K_2(t) = \text{diag}(k_{12}, k_{22})$, and $K_3(t) = \text{diag}(k_{13}, k_{23}, k_{33})$ are diagonal time-varying matrices, in which k_{ij} will be designed to achieve the acceptable convergence time. Besides, $f_{1a}(t, \hat{x}) = [\hat{y}, -\frac{b}{m}\hat{y} + \frac{A_P P_L}{m}, 0]^T$, $f_{2a}(t, \hat{x}) = f_{2a}(t, x)$, and $f_{3a}(t, \hat{x}) = [\hat{v}_e, -\omega_{nv}^2 v_e - 2\epsilon_v \omega_{nv} \hat{v}_e, 0]^T$.

Now according to (10)-(12), by defining the observation error $e = x_a(t) - \hat{x}_a(t)$, the following error dynamics are achieved:

$$\dot{e}_1(t) = A_1 e_1 + B_1 \dot{\phi}_1(t, x) \quad (13)$$

$$\dot{e}_2(t) = A_2 e_2 + B_2 \dot{\phi}_2(t, x) \quad (14)$$

$$\dot{e}_3(t) = A_3 e_3 + B_3 \dot{\phi}_3(t, x) \quad (15)$$

$$\text{where } A_1 = \begin{bmatrix} -k_{11} & 1 & 0 \\ -k_{21} & -\frac{b}{m} & 1 \\ -k_{31} & 0 & 0 \end{bmatrix}, \quad A_2 = \begin{bmatrix} -k_{12} & 1 \\ -k_{22} & 0 \end{bmatrix}, \quad \text{and}$$

$$A_3 = \begin{bmatrix} -k_{13} & 1 & 0 \\ -k_{23} & -2\epsilon_v \omega_{nv} & 1 \\ -k_{33} & 0 & 0 \end{bmatrix}. \quad \text{Now, to}$$

investigate the finite-time stability of error dynamics (13)-(15), the time-varying gains k_{ij} should be designed. In this regard, Theorem 1 is presented.

Theorem 1. Consider the observation error dynamics (13)-(15). If the scalar coefficients L_{ij} for $i = 1, \dots, n_j$ and $j = 1, 2$, and 3, are chosen such that the $n_j \times$

$$n_j \text{ matrix } \Theta_{oj} = \begin{bmatrix} -L_{1j} & I_{n_j-1} \\ \vdots & \\ -L_{n_j j} & 0 \end{bmatrix} \text{ is}$$

Hurwitz, then the observation errors tend

to a small neighborhood around zero in a finite time by defining the observer gains k_{ij} as

$$k_{11} = L_{11} + \frac{n_1 \dot{\mu}}{\mu} - \bar{k}_{21(1)} \mu \quad (16)$$

$$k_{21} = L_{21} + \frac{n_1 \dot{\mu}}{\mu} - \bar{k}_{21(1)}^2 \mu^2 + \bar{k}_{21(1)} \left(\dot{\mu} + n_1 \dot{\mu} - \mu k_{11} + \frac{b}{m} \mu \right) \quad (17)$$

$$k_{31} = L_{31} + \frac{n_1 \dot{\mu}}{\mu} \quad (18)$$

where $\bar{k}_{21(1)} = \frac{b}{m} \mu^{-1}$. Also, the observer gains of the second subsystem are defined as

$$k_{12} = L_{12} + \frac{n_2 \dot{\mu}}{\mu} \quad (19)$$

$$k_{22} = L_{22} + \frac{n_2 \dot{\mu}}{\mu} \quad (20)$$

and then for $\bar{k}_{21(3)} = 2\epsilon_v \omega_{nv} \mu^{-1}$, the observer gains of the third subsystem are

$$k_{13} = L_{13} + \frac{n_3 \dot{\mu}}{\mu} - \bar{k}_{21(3)} \mu \quad (21)$$

$$k_{23} = L_{23} + \frac{n_3 \dot{\mu}}{\mu} - \bar{k}_{21(3)}^2 \mu^2 + \bar{k}_{21(3)} (\dot{\mu} + n_3 \dot{\mu} - \mu k_{13} + 2\epsilon_v \omega_{nv} \mu) \quad (22)$$

$$k_{33} = L_{33} + \frac{n_3 \dot{\mu}}{\mu} \quad (23)$$

so that there exist positive constants $c_j > 1$, to make the observation error dynamics (13)-(15) FT-ISS as,

$$\begin{aligned} & \|e_j\| \\ & \leq v \sup_t \|\tilde{K}_j(v)\| \left[c_j \exp(\Theta_{oj} t) \|\bar{K}_j(1)\| \|e_j(0)\| \right. \\ & \quad \left. + \int_0^t \exp(\Theta_{oj}(t - \tau)) \mu^{n_j} |\dot{\phi}_j(t, x(t))| d\tau \right] \end{aligned} \quad (24)$$

where $\mu = \frac{1+e^{-\frac{t}{\varrho}}}{2e^{-\frac{t}{\varrho}}}$ and $v = \mu^{-1}$ are positive time-varying functions. Also,

$\bar{K}_j(\mu)$ is lower triangular $n_j \times n_j$ matrix, where $\bar{K}_1(\mu)$ is defined in the form of (25), $\bar{K}_2(\mu) = \text{diag}(\mu, \mu)$ and $\bar{K}_3(\mu) = \text{diag}(\mu^2, \mu^2, \mu^2)$. Besides, $\bar{K}_j(1)$ s are the matrices $\bar{K}_j(\mu)$ s at the time $t = 0$, and $\tilde{K}_j(v)$ is defined as $\bar{K}_j(\mu_1)^{-1}$, where $\bar{K}_j(\mu)\tilde{K}_j(v) = I$.

$$\bar{K}_1(\mu) = \begin{bmatrix} \mu^2 & 0 & 0 \\ \bar{k}_{2,1(j)}\mu^3 & \mu^2 & 0 \\ 0 & 0 & \mu^2 \end{bmatrix} \quad (25)$$

Proof. The present proof is constructed based on Remark 1. Consider the following primary transformation $e \rightarrow \omega$

$$\omega_j = \mu^{n_j} e_i \quad (26)$$

where $j = 1, 2$, and 3 . The derivatives of ω_j s along with the observation error dynamics (13)-(15) are as

$$\dot{\omega}_1 = A_{1a}\omega_1 + B_1 \mu^{n_1} \dot{\phi}_1(t, x(t)) \quad (27)$$

$$\dot{\omega}_2 = A_{2a}\omega_2 + B_2 \mu^{n_2} \dot{\phi}_2(t, x(t)) \quad (28)$$

$$\dot{\omega}_3 = A_{3a}\omega_3 + B_3 \mu^{n_3} \dot{\phi}_3(t, x(t)) \quad (29)$$

where A_{ja} s are as

$$\begin{aligned} A_{1a} &= \begin{bmatrix} \frac{n_1\dot{\mu}}{\mu} - k_{11} & 1 & 0 \\ \frac{n_1\dot{\mu}}{\mu} - k_{21} & -\frac{b}{m} & 1 \\ \frac{n_1\dot{\mu}}{\mu} - k_{31} & 0 & 0 \end{bmatrix} \\ A_{2a} &= \begin{bmatrix} \frac{n_2\dot{\mu}}{\mu} - k_{12} & 1 \\ \frac{n_2\dot{\mu}}{\mu} - k_{22} & 0 \end{bmatrix} \\ A_{3a} &= \begin{bmatrix} \frac{n_3\dot{\mu}}{\mu} - k_{13} & 1 & 0 \\ \frac{n_3\dot{\mu}}{\mu} - k_{23} & -2\epsilon_v\omega_{nv} & 1 \\ \frac{n_3\dot{\mu}}{\mu} - k_{33} & 0 & 0 \end{bmatrix} \end{aligned} \quad (30)$$

Besides, for $i = 1, \dots, n_j$ and $j = 1, 2$, and 3 , the following secondary transformation $\omega \rightarrow z$ is defined,

$$z_{i(j)} = \sum_{\gamma=1}^i \bar{k}_{i,\gamma(j)} \mu^{i-\gamma} \omega_{\gamma(j)} \quad (31)$$

where $\bar{k}_{i,i(j)} = 1$, and for $i < \gamma$ one has $\bar{k}_{i,\gamma(j)} = 0$, as well as $\bar{k}_{3,1(1)} = \bar{k}_{3,2(1)} = \bar{k}_{2,1(0)} = 0$; wherein $\omega_{\gamma(j)}$ and (j) represent the element γ of vector ω_j and the number of each subsystem, respectively. Therefore,

$$\begin{aligned} \dot{z}_{i(j)} &= \sum_{\gamma=1}^i \bar{k}_{i,\gamma(j)} \mu^{i-\gamma} \dot{\omega}_{\gamma(j)} \\ &\quad + \sum_{\gamma=1}^i \bar{k}_{i,\gamma(j)} (i - \gamma) \mu^{i-\gamma-1} \dot{\mu} \omega_{\gamma(j)} \end{aligned} \quad (32)$$

By substituting (26)-(31) into (32) it can be easily shown that

$$\begin{aligned} \dot{z}_{1(1)} &= \left[-k_{11} - \bar{k}_{21(1)}\mu + \frac{n_1\dot{\mu}}{\mu} \right] z_{1(1)} \\ &\quad + z_{2(1)} \end{aligned}$$

$$\begin{aligned} \dot{z}_{2(1)} &= \left[-k_{21} - \bar{k}_{21(1)}^2 \mu^2 \right. \\ &\quad + \bar{k}_{21(1)} \left(\dot{\mu} + n_1 \dot{\mu} - k_{11}\mu + \frac{b}{m}\mu \right) \\ &\quad + \bar{k}_{21(1)} \bar{k}_{32(1)} \mu^2 - \bar{k}_{31(1)} \mu^2 \\ &\quad \left. + \frac{n_1\dot{\mu}}{\mu} \right] z_{1(1)} \\ &\quad + \left[\bar{k}_{21(1)}\mu - \bar{k}_{32(1)}\mu - \frac{b}{m} \right] z_{2(1)} + z_{3(1)} \end{aligned}$$

$$\begin{aligned}
\dot{z}_{3(1)} &= \left[-k_{31} - \bar{k}_{21(1)} \bar{k}_{31(1)} \mu^3 \right. \\
&+ \bar{k}_{21(1)} \bar{k}_{32(1)} \left(\bar{k}_{32(1)} \mu^3 - \mu \dot{\mu} \right. \\
&+ \left. \frac{b}{m} \mu^2 \right) + \bar{k}_{31(1)} (2\mu \dot{\mu} - \bar{k}_{32(1)} \mu^3) \\
&+ \left. \bar{k}_{32(1)} (n_1 \dot{\mu} - k_{21} \mu) + \frac{n_1 \dot{\mu}}{\mu} \right] z_{1(1)} \\
&+ \left[\bar{k}_{31(1)} \mu^2 \right. \\
&+ \left. \bar{k}_{32(1)} \left(\dot{\mu} - \frac{b}{m} \mu - \mu^2 \right) \right] z_{2(1)} \\
&+ \left[\bar{k}_{32(1)} \mu \right] z_{3(1)} + \mu^{n_1} \dot{\phi}_1(t, x(t))
\end{aligned}$$

and

$$\begin{aligned}
\dot{z}_{1(2)} &= \left[-k_{12} - \bar{k}_{21(2)} \mu + \frac{n_2 \dot{\mu}}{\mu} \right] z_{1(2)} \\
&+ z_{2(2)} \\
\dot{z}_{2(2)} &= \left[-k_{22} \right. \\
&+ \bar{k}_{21(2)} (\dot{\mu} \\
&+ n_2 \dot{\mu} - k_{12} \mu - \mu^2) \\
&+ \left. \frac{n_2 \dot{\mu}}{\mu} \right] z_{1(2)} \\
&+ \left[\bar{k}_{21(2)} \mu \right] z_{2(2)} \\
&+ \mu^{n_2} \dot{\phi}_2(t, x(t))
\end{aligned}$$

and

$$\begin{aligned}
\dot{z}_{1(3)} &= \left[-k_{13} - \bar{k}_{21(3)} \mu + \frac{n_3 \dot{\mu}}{\mu} \right] z_{1(3)} \\
&+ z_{2(3)} \\
\dot{z}_{2(3)} &= \left[-k_{23} - \bar{k}_{21(3)}^2 \mu^2 \right. \\
&+ \bar{k}_{21(3)} (\dot{\mu} + n_3 \dot{\mu} \\
&- k_{13} \mu + 2\epsilon_v \omega_{nv} \mu) \\
&+ \bar{k}_{21(3)} \bar{k}_{32(3)} \mu^2 \\
&- \bar{k}_{31(3)} \mu^2 \\
&+ \left. \frac{n_3 \dot{\mu}}{\mu} \right] z_{1(3)} \\
&+ \left[\bar{k}_{21(3)} \mu - \bar{k}_{32(3)} \mu \right. \\
&- \left. 2\epsilon_v \omega_{nv} \right] z_{2(3)} + z_{3(3)}
\end{aligned}$$

$$\begin{aligned}
\dot{z}_{3(3)} &= \left[-k_{33} - \bar{k}_{21(3)} \bar{k}_{31(3)} \mu^3 \right. \\
&+ \bar{k}_{21(3)} \bar{k}_{32(3)} (\bar{k}_{32(3)} \mu^3 - \mu \dot{\mu} \\
&+ 2\epsilon_v \omega_{nv} \mu^2) \\
&+ \bar{k}_{31(3)} (2\mu \dot{\mu} - \bar{k}_{32(3)} \mu^3) \\
&+ \bar{k}_{32(3)} (n_3 \dot{\mu} - k_{23} \mu) + \left. \frac{n_3 \dot{\mu}}{\mu} \right] z_{1(3)} \\
&+ \left[\bar{k}_{31(3)} \mu^2 \right. \\
&+ \left. \bar{k}_{32(3)} (\dot{\mu} - 2\epsilon_v \omega_{nv} \mu - \mu^2) \right] z_{2(3)} \\
&+ \left[\bar{k}_{32(3)} \mu \right] z_{3(3)} + \mu^{n_3} \dot{\phi}_3(t, x(t))
\end{aligned}$$

Then, by choosing the gains according to (16)-(23), it is obtained that

$\dot{z}_{i(j)} = \theta_{oj} z_{i(j)} + B_j \mu^{n_j} \dot{\phi}_j(t, x(t))$ where θ_{oj} and B_j have already been defined. Now, by choosing the scalar coefficients L_{ij} for $i = 1, \dots, n_j$ and $i = 1, 2$, and 3, to make the matrices θ_{oj} Hurwitz, there exist positive constants $c_j > 1$, such that,

$$\begin{aligned}
&\|z_{i(j)}\| \\
&\leq \varepsilon \exp(\theta_{oj} t) \|z_{i(j)}(0)\| \\
&+ \int_0^t \exp(e^{\theta_{oj}(t-\tau)}) \mu^{n_j} |\dot{\phi}_j(t, x(t))| d\tau
\end{aligned} \tag{33}$$

Now, combining the transformations (26) and (31) leads to

$$z_{i(j)} = \mu \bar{K}_j(\mu) e_{i(j)} \tag{34}$$

where its inverse is defined as follows,

$$e_{i(j)} = v \tilde{K}_j(v) z_{i(j)}$$

consequently,

$$\|e_{i(j)}\| \leq v \sup_t \|\tilde{K}_j(v)\| \|z_{i(j)}\| \tag{35}$$

Moreover, based on the transformation (34), one has

$$\|z_{i(j)}(0)\| \leq \|\bar{K}_j(1)\| \|e_{i(j)}(0)\| \tag{36}$$

where $\bar{K}_j(1)$ is the matrix $\bar{K}_j(\mu)$ at the time $t = 0$. Then, by substituting (36) into (33) and subsequently substituting into (35) the result (24) is achieved. As a

result, since $\bar{K}_j(\mu)$ is a positive definite matrix for any $t \geq 0$, the greatest lower bound of $\bar{K}_j(\mu)$ (i.e. $\inf_t |\bar{K}_j(\mu)|$) exists and consequently $\sup_t |\tilde{K}_j(v)|$ is bounded.

Therefore, according to Remark 1, if the right-hand side of the inequality (24) (except v) remains bounded, based on the time-varying variable v , it is clear that $e_{i(j)}$ will tend to the neighborhood of zero and will remain uniformly bounded in a finite time. Since $|\dot{\phi}_j(t, x(t))|$ has been bounded so $\int_0^t \exp(\theta_{oj}(t - \tau)) \mu^{n_j} |\dot{\phi}_j(t, x(t))| d\tau$ is bounded. Besides, $c_j \exp(\theta_{oj} t) \|\bar{K}_j(1)\| \|e_j(0)\|$ for small initial conditions would be bounded. Therefore, according to the definitions 1 and 2, the boundedness of the observation errors $e_{i(j)}$ is guaranteed; thus, the arguments stated in Theorem 1 hold. This ruling completes the proof. \square

3.2. Implementation Issues

One concern of the introduced scheme is the definition of the time-varying transformation μ , since it can tend to infinity when $t \rightarrow \infty$. Although μ tends to infinity, but $t = \infty$ will not happen in real-life applications. However, to overcome this concern, its definition can be modified as,

$$\mu = \begin{cases} \frac{1+e^{-\frac{t}{\delta_t}}}{2e^{-\frac{t}{\delta_t}}} & t \leq \delta_t \\ \mu_{Max} & t > \delta_t \end{cases} \quad (37)$$

where for a positive real constant δ_t , the constant μ_{Max} is defined as $1 + e^{-\frac{\delta_t}{\delta_t}} / 2e^{-\frac{\delta_t}{\delta_t}}$. The constant δ_t should be designed based on a trade-off between the observation errors and the convergence time. It is worth noting that the designed observer provides acceptable values for the states in a finite time, before any diverging effect. In order to adapt the stability proofs to this new definition (37), we consider two time intervals $t \leq \delta_t$ and $t > \delta_t$ to

perform the analysis. For the first one, the previous proofs are valid. Also, since we have already proved that the observed states remain within the ball in a finite time, and remain bounded at all times, therefore this statement will remain valid for the second time interval.

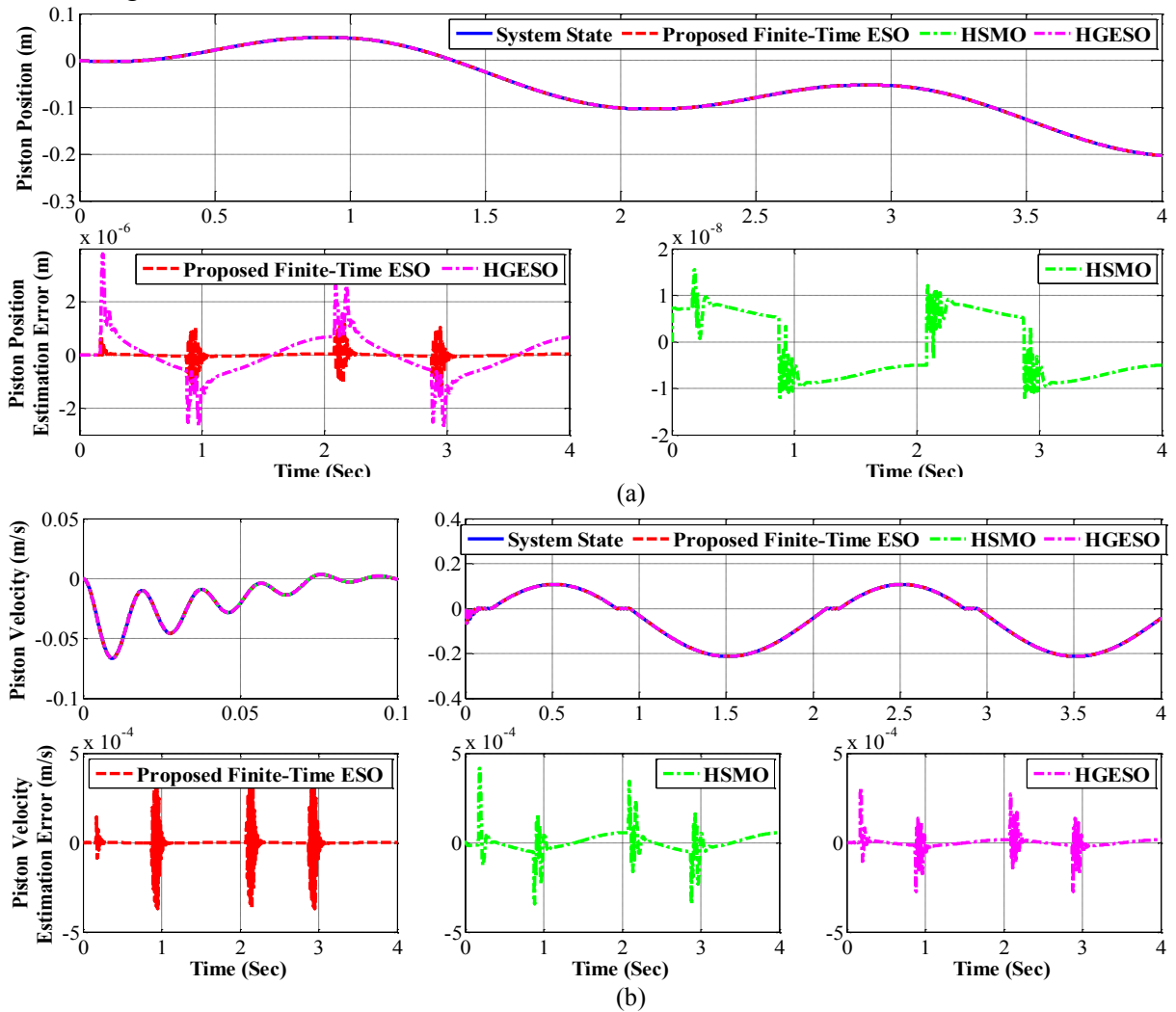
Remark 3. In this paper, the diagonal time-varying matrices $K_1(t)$, $K_2(t)$, and $K_3(t)$ consist of k_{ij} s that should be designed as (16)-(23) to achieve the acceptable convergence time and in line with guaranteeing the Hurwitz condition for matrices θ_{oj} . The proposed scheme is straightforward to design and realize. Its construction relies only on choosing the constants L_{1j}, \dots, L_{1j} (for $j = 1, 2, 3$), to make the matrices θ_{oj} Hurwitz, and then choosing the constants ρ and δ_t , independently, where increasing the value of ρ increases the convergence time considerably and vice versa. Also, the constant δ_t should be designed based on a trade-off between singularity problem, the finite-time efficiency and the observation errors. To guarantee the estimation in a finite time, δ_t is proposed as a positive high-value constant, where increasing its value significantly decreases the convergence time and considerably reduces the observation errors.

4. Computer Simulations

In this Section, to highlight the efficiency of the proposed finite-time ESO, several comparative simulations are reported compared to the two leading strategies HSMO [15] and HGESO [27]. Then, further simulations are reported to validate the performance of the proposed framework in the presence of measurement noise. The parameters for the observers are the same as the EHA's parameters, with the explicit values provided in [15]. In this Section, without loss of generality, the estimation word is sometimes used for observation purposes. The simulation results are achieved under zero-initial conditions for

all state variables. To understand the dead-zone's effects, the results are obtained by employing a low-frequency sine wave $u = 2\sin(\pi t)$. The performance analysis of the proposed finite-time ESO is shown in Fig. 2 for the first subsystem. From this plot, the following three considerations can be drawn: (1) Finite-time convergence is achieved. Fig. 2 shows the time evolutions of state variables of the first subsystem and their estimations, in which the proposed scheme has obtained an acceptable convergence time compared with HSMO and HGESO; (2) The proposed finite-time ESO results in the proper estimation of the state variables, as well as the uncertainties, whose observation errors converge to a small neighborhood of zero. Thus, the proposed approach is an alternative way to design the disturbance observers.

Especially, Fig. 2(c) shows that the proposed finite-time ESO achieves comparable estimation performance with respect to HSMO and HGESO, even in the presence of external force such as friction force and disturbance that was defined as an uncertainty in the EHA; (3) Fig. 2 show that the external force and subsequently the friction force $F_f(\dot{y})$ and then $\varphi_1(t, x)$ are continuous and bounded. Inspired by preliminaries of a version of Barbalat-like lemma [33], it can be concluded that the continuity of $\varphi_1(t, x)$ guarantees the assumed condition $|\dot{\varphi}_1(t, x)| \leq \sigma_1$; hence the arguments stated in Section 2 hold. The performance of the studied approaches in terms of the Root Mean Square (RMS) values of the observation errors are calculated in Table 1.



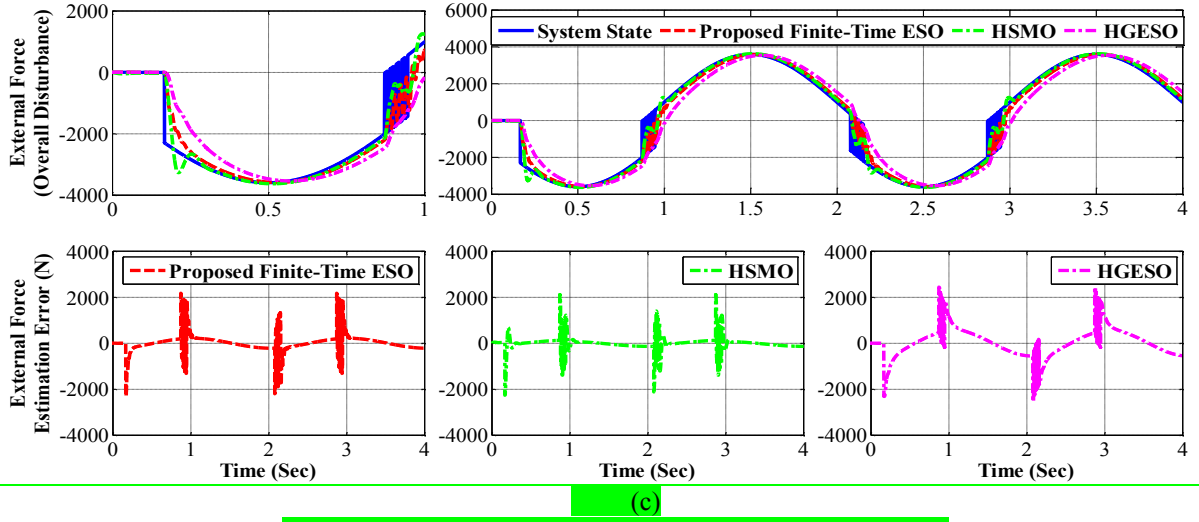


Fig. 2 Real states and estimation results of the first subsystem.

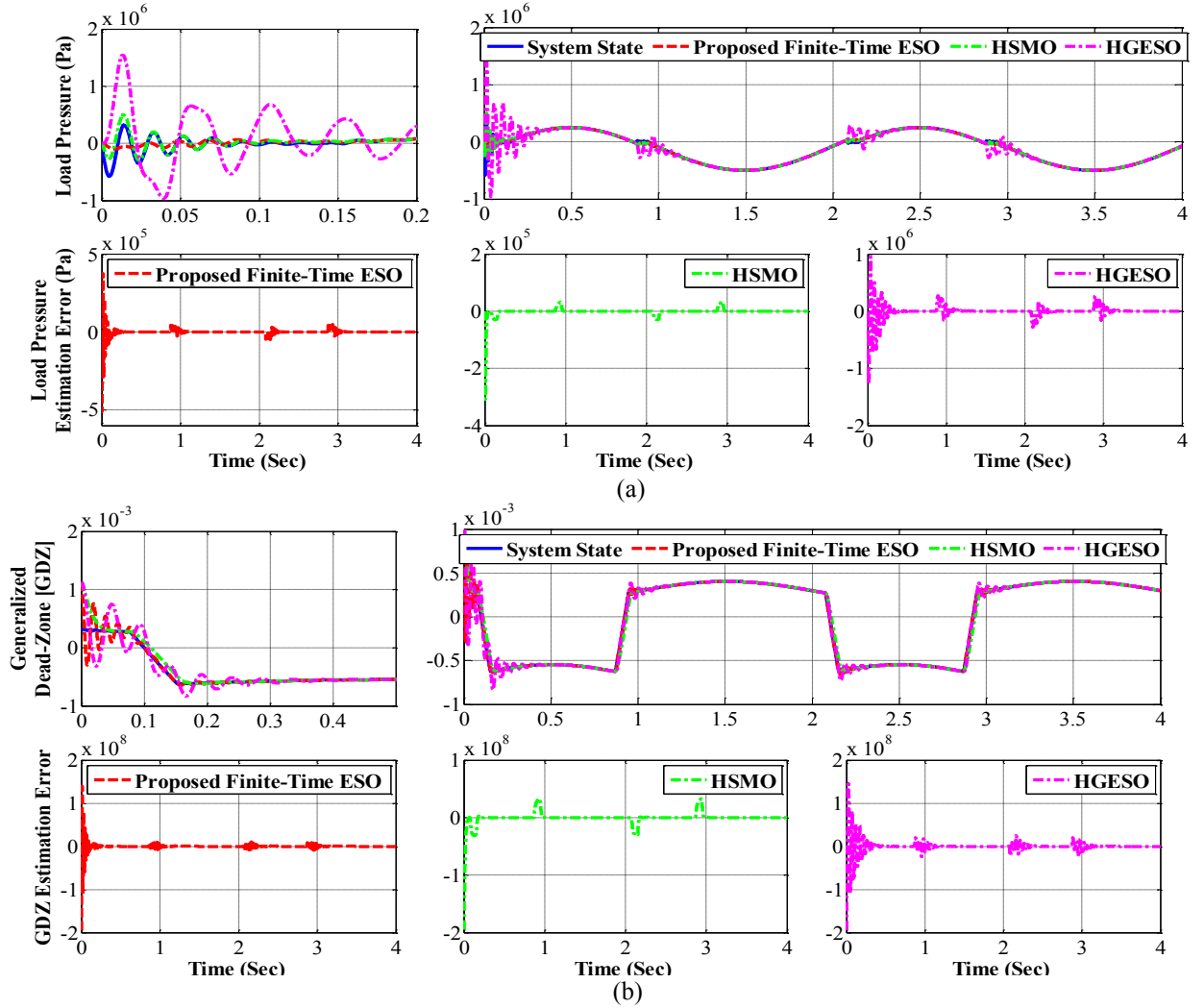


Fig. 3. Real states and estimation results of the second subsystem.

A performance index is defined based on the RMS of the observation error

vector e_1 , as $J_1 = \left\| \sqrt{\frac{1}{t_s} \int_0^{t_s} e_1^T e_1 dt} \right\|$, where $t_s = 4$ is the simulation time.

Table 1

Comparative results between the first-subsystem performance indexes.

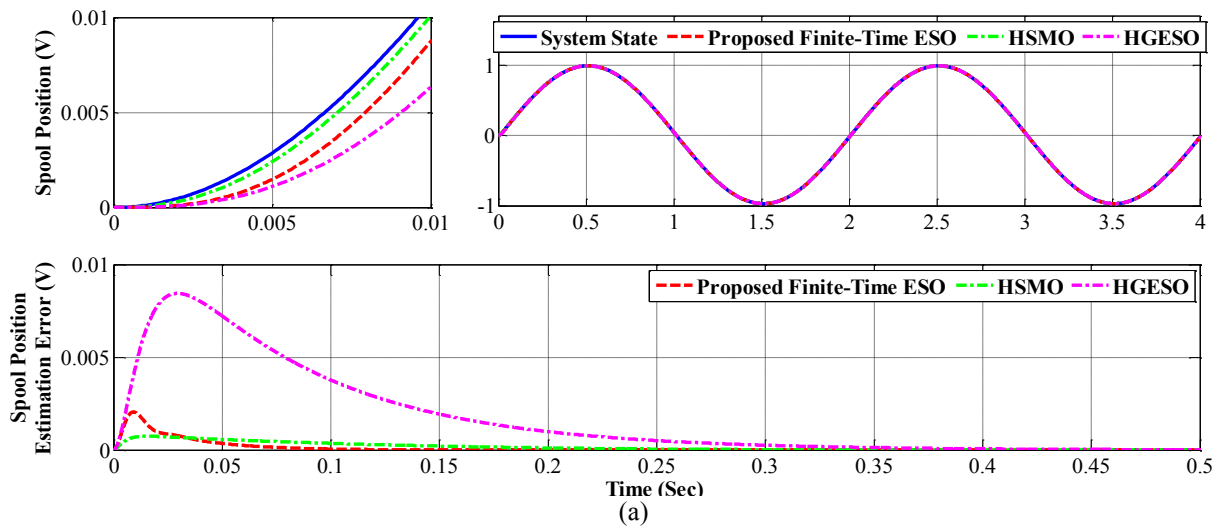
Methods	Quantity of performance indexes
Proposed finite-time ESO	$J_1 = \begin{bmatrix} 4.349E-12 \\ 1.354E-7 \\ 783.162 \end{bmatrix}$
HSMO [15]	$J_1 = \begin{bmatrix} 3.437E-14 \\ 5.024E-7 \\ 783.162 \end{bmatrix}$
HGESO [27]	$J_1 = \begin{bmatrix} 7.814E-11 \\ 1.949E-7 \\ 759.238 \end{bmatrix}$

It is worth noting that, in order to produce a fair analysis, the parameters for the proposed comparison with HSMO and HGESO are taken directly from [15] and [27] with their highest efficiency. Table 1 confirms that the proposed ESO can compete with HSMO and HGESO approaches as leading strategies.

The second subsystem is affected by uncertainties coming from subsystems 1 and 3. Fig. 3 shows that the proposed observer ensures a similar convergence time as HSMO and HGESO. The proposed finite-time ESO results in the appropriate estimation of the state variables as well as the uncertainties. In particular, Fig. 3(b) shows that the proposed scheme achieves great estimation performance, even in the

presence of Dead-Zone effects. It is worth noting that, according to Fig. 3, there is no significant difference between the convergence times, and the obtained results are almost similar. By defining the RMS performance index $J_2 = \left\| \sqrt{\frac{1}{t_s} \int_0^{t_s} e_2^T e_2 dt} \right\|$, it can be shown that its value for all three methods is 800, confirming that the proposed ESO can compete with HSMO and HGESO approaches.

As noted in Section 2, the third subsystem represents the proportional valve dynamics, which is one-side-independent of the other subsystems. Finite-time convergence and disturbance estimation considerations for this subsystem are shown in Fig. 4. Especially, Fig. 4(c) shows that comparable estimation performance with respect to HSMO and HGESO is achieved in the presence of unknown terms $\omega_{nv}^2 v_{e0} + \eta_{v_e}(t)$. By defining the RMS performance index $J_3 = \left\| \sqrt{\frac{1}{t_s} \int_0^{t_s} e_3^T e_3 dt} \right\|$, based on the infinity norm of the observation error vector e_3 , the performance of all three observers is evaluated in Table 2.



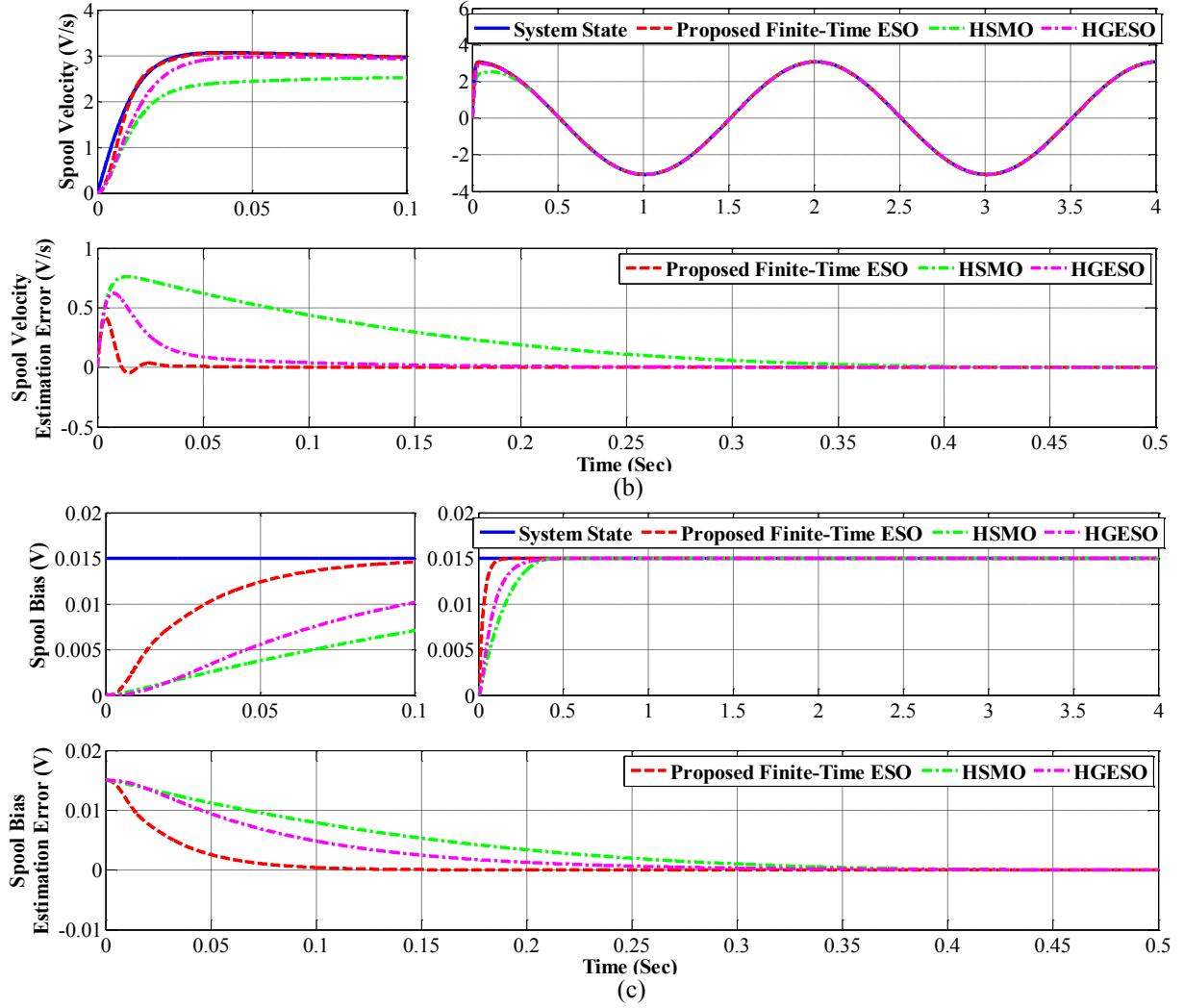


Fig. 4. Real states and estimation results of the third subsystem.

Table 2

Comparative results between the third-subsystem performance indexes.

Methods	Quantity of performance indexes
Proposed finite-time ESO	$J_3 = \begin{bmatrix} 2.009E-6 \\ 0.0457 \\ 799.9845 \end{bmatrix}$
HSMO [15]	$J_3 = \begin{bmatrix} 1.8400E-6 \\ 2.3822 \\ 799.9845 \end{bmatrix}$
HGESO [27]	$J_3 = \begin{bmatrix} 2.1965E-6 \\ 0.3166 \\ 799.9845 \end{bmatrix}$

We conclude that the finite-time convergence is guaranteed without any knowledge about the upper bounds of the disturbances. Therefore, the proposed scheme can compete with the other two leading strategies, which makes it a qualified alternative approach in the

observer design with noteworthy potential. Besides, Figs. 3(b) and 4(c) show that $\varphi_2(t, x)$ and $\varphi_3(t, x)$ are continuous and bounded; where their continuity guarantees the assumed conditions $|\dot{\varphi}_2(t, x)| \leq \sigma_2$ and $|\dot{\varphi}_3(t, x)| \leq \sigma_3$.

On the other hand, in practice, exact measurements as the ones considered in the previous simulation are impossible to obtain. In real life, sensor data are affected by external noise, therefore, the effectiveness of the proposed observer should be evaluated in the presence of unknown measurement noise. Assume that the outputs are redefined as $z(t) = [y + N_1(t), P_L + N_2(t), v_e + N_3(t)]^T$, where $N_i(t)$ for $i = \{1, 2, 3\}$ are unknown band-limited white noises. Since the HGESO is basically an

approximate differentiator, measurement noise and unmodeled high-frequency dynamics will put a practical limit on its use [32]. In this Section, without loss of generality, the simulated performance of the presented framework is only

compared with HSMO approach. The performance of the proposed scheme is validated in the presence of measurement noise. Fig. 5(c) shows that the external force is well estimated, even in the presence of measurement noise.

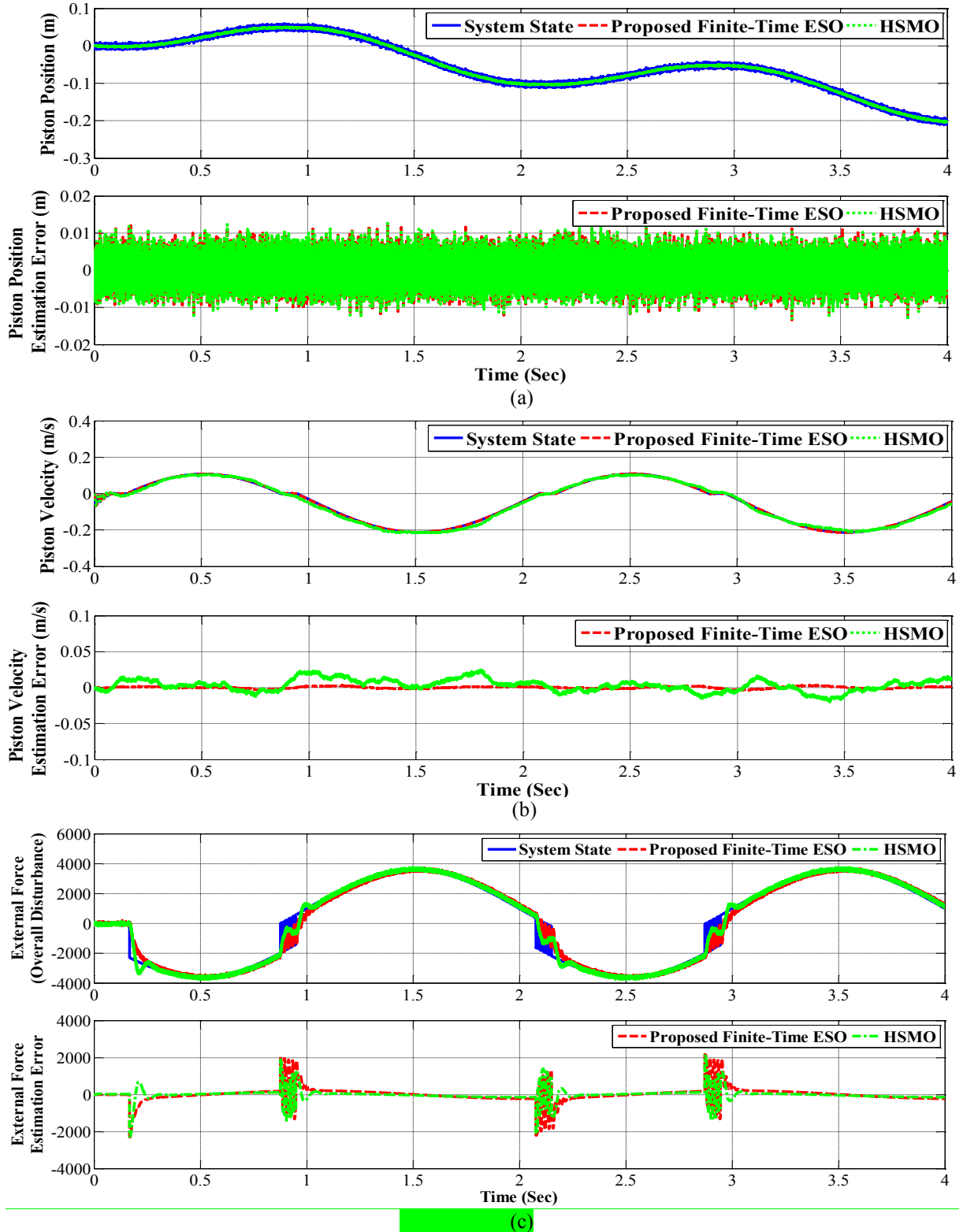


Fig. 5. Real states and estimation results of the first subsystem under measurement noise.

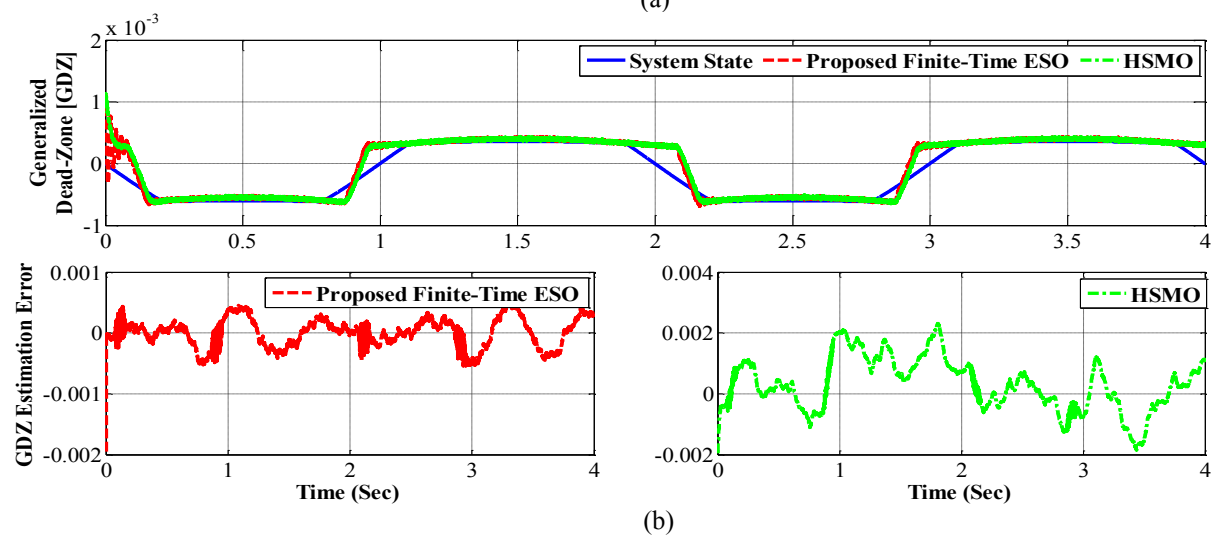
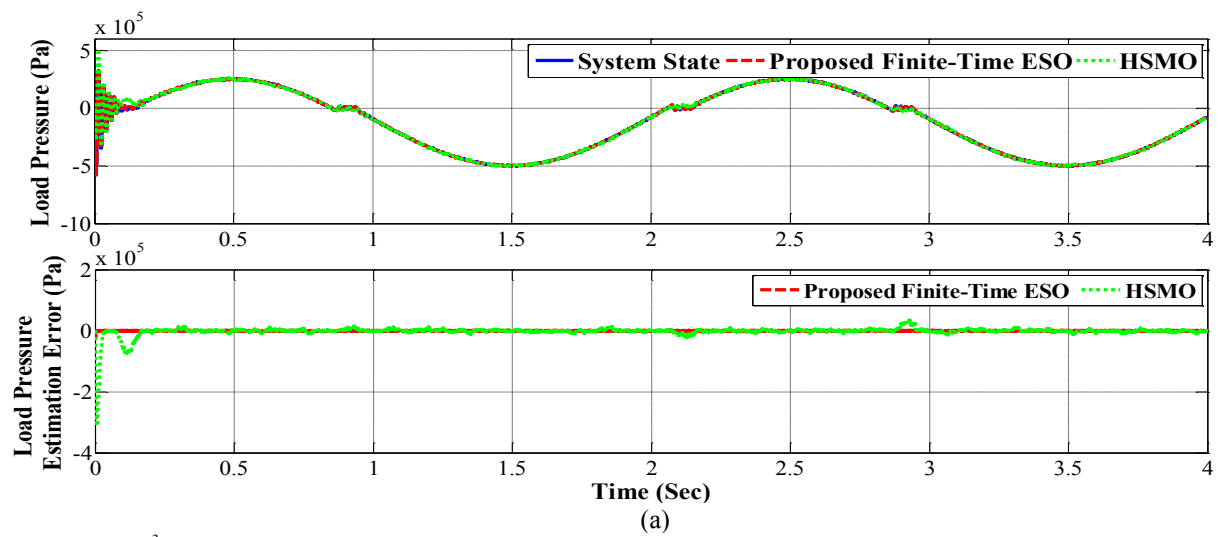
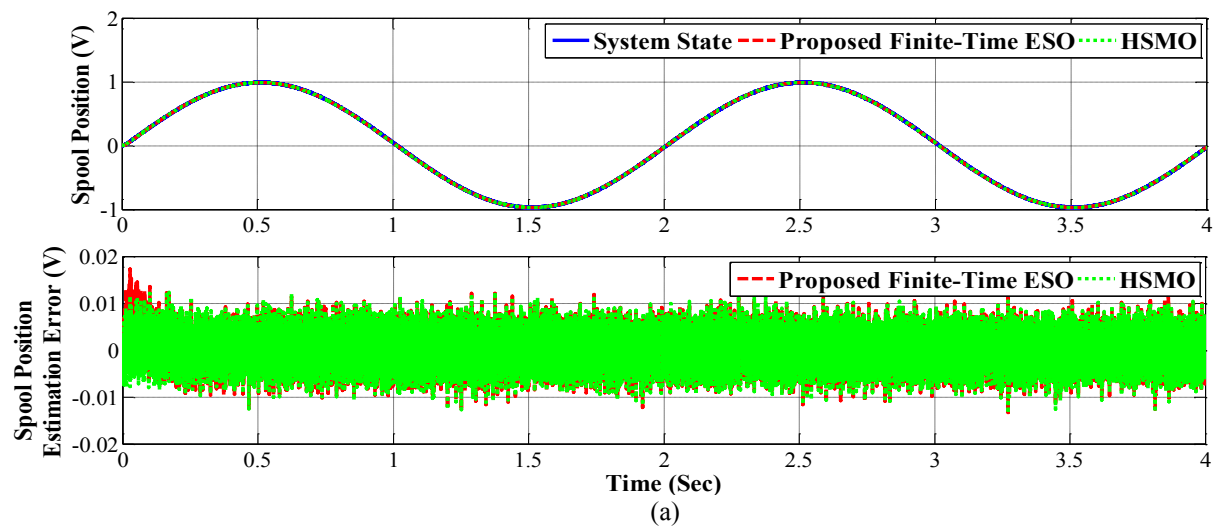


Fig. 6. Real states and estimation results of the second subsystem under measurement noise.



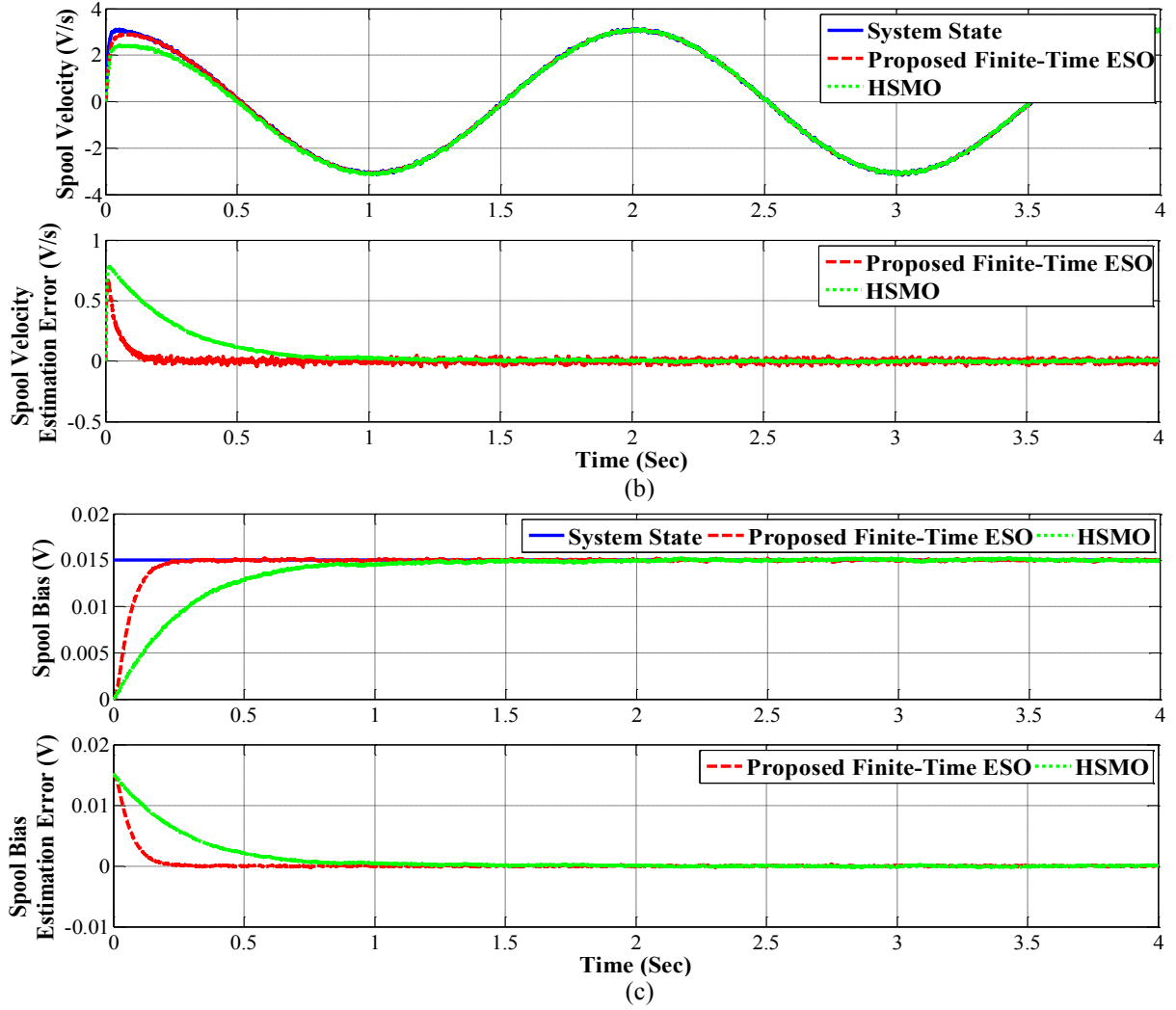


Fig. 7. Real states and estimation results of the third subsystem under measurement noise.

Fig. 6 shows that the proposed framework has an acceptable convergence time compared with HSMO. Besides, Fig. 6(b) shows that the proposed scheme achieves great estimation performance, even in the presence of Dead-Zone effects as well as measurement noise. According to Fig. 7, the acceptable performance of the proposed scheme is achieved in the presence of measurement noise as well as uncertainties. Besides, the difference between convergence times is quite obvious; hence, the efficiency of the proposed scheme is confirmed as a practical method in the presence of measurement noise.

5. Experimental Results

Experimental results are obtained on the EHA test-bed shown in Fig. 8. The setup is equipped with sensors providing measurements of output variables y , P_L , and v_e . Besides, in comparison with the data estimated by the observers, these practical data are first reconstructed through digital filtering. In this paper, to validate the effectiveness of the proposed finite-time ESO in a real-life scenario, an experiment in presence of a load connected to the sliding table is performed; where markers 1 to 6 respectively indicate the fixed base, sliding table, isolator under test, an external load, numerical computer, and power supply. In the experimental tests, the supply pressure P_s is less than the one used in simulations. The proposed

scheme is straightforward to design and implement. Its construction relies only on the selection of the constants L_{ij} to make the matrix θ_{oj} Hurwitz, and then the selection of the constants ϱ and δ_t , independently. Therefore, without any singularity and chattering concerns, the proposed observer scheme is useful as a practical and alternative approach for states and uncertainties observation.

Figs. 9–11 show the comparative experimental results. By considering the convergence time and amplitude of results, it is seen that the response of HGESO is not as strong as the other two methods.

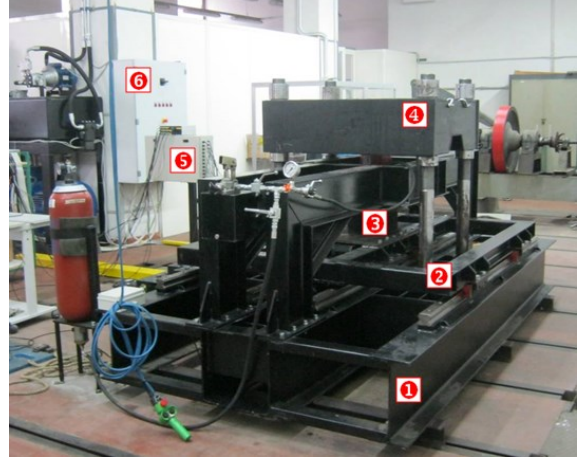
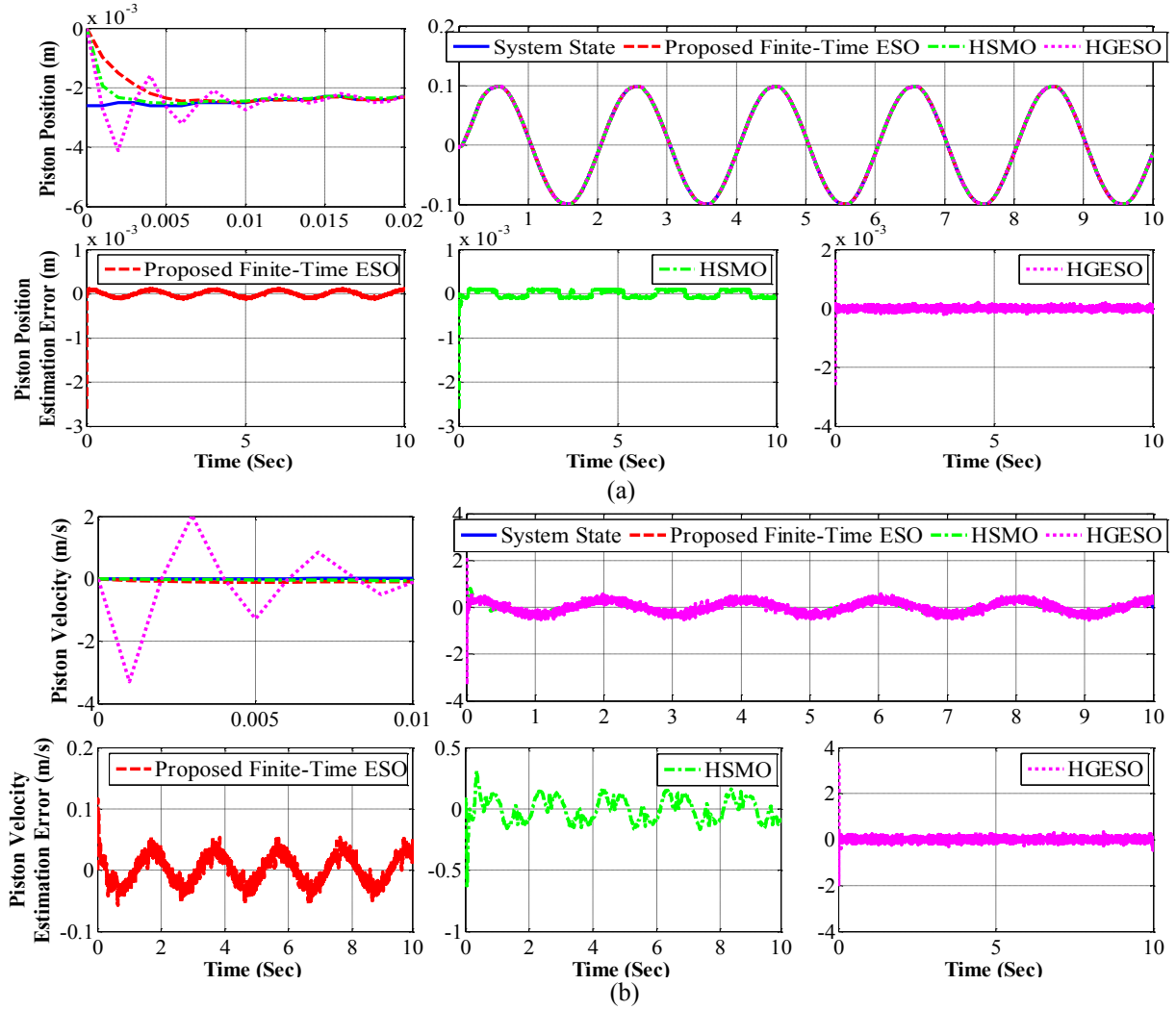
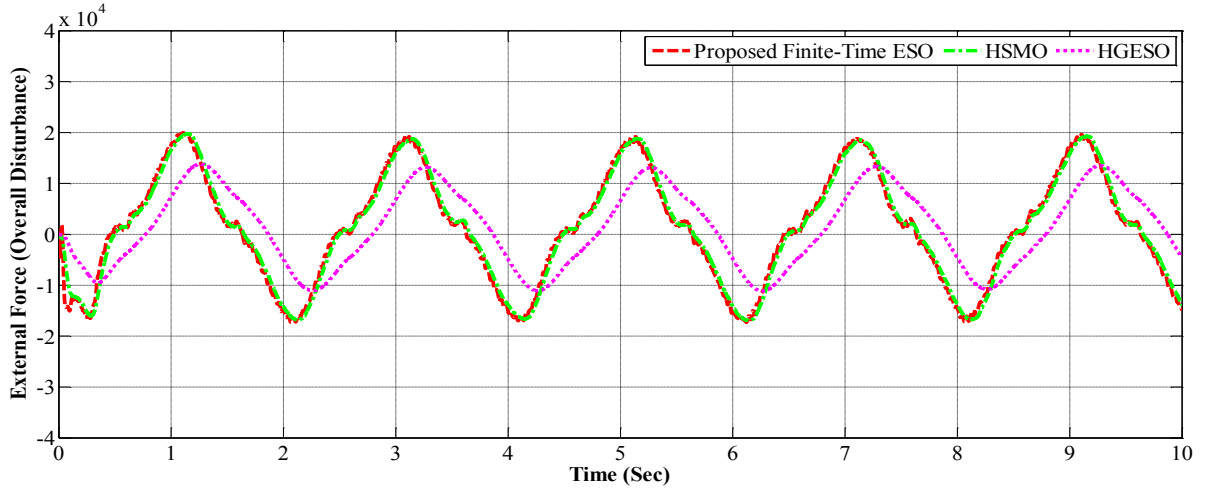


Fig. 8. The EHA test-bed used during the experiments.





(c)
Fig. 9. Real states and estimation results of the first subsystem (Experimental results).

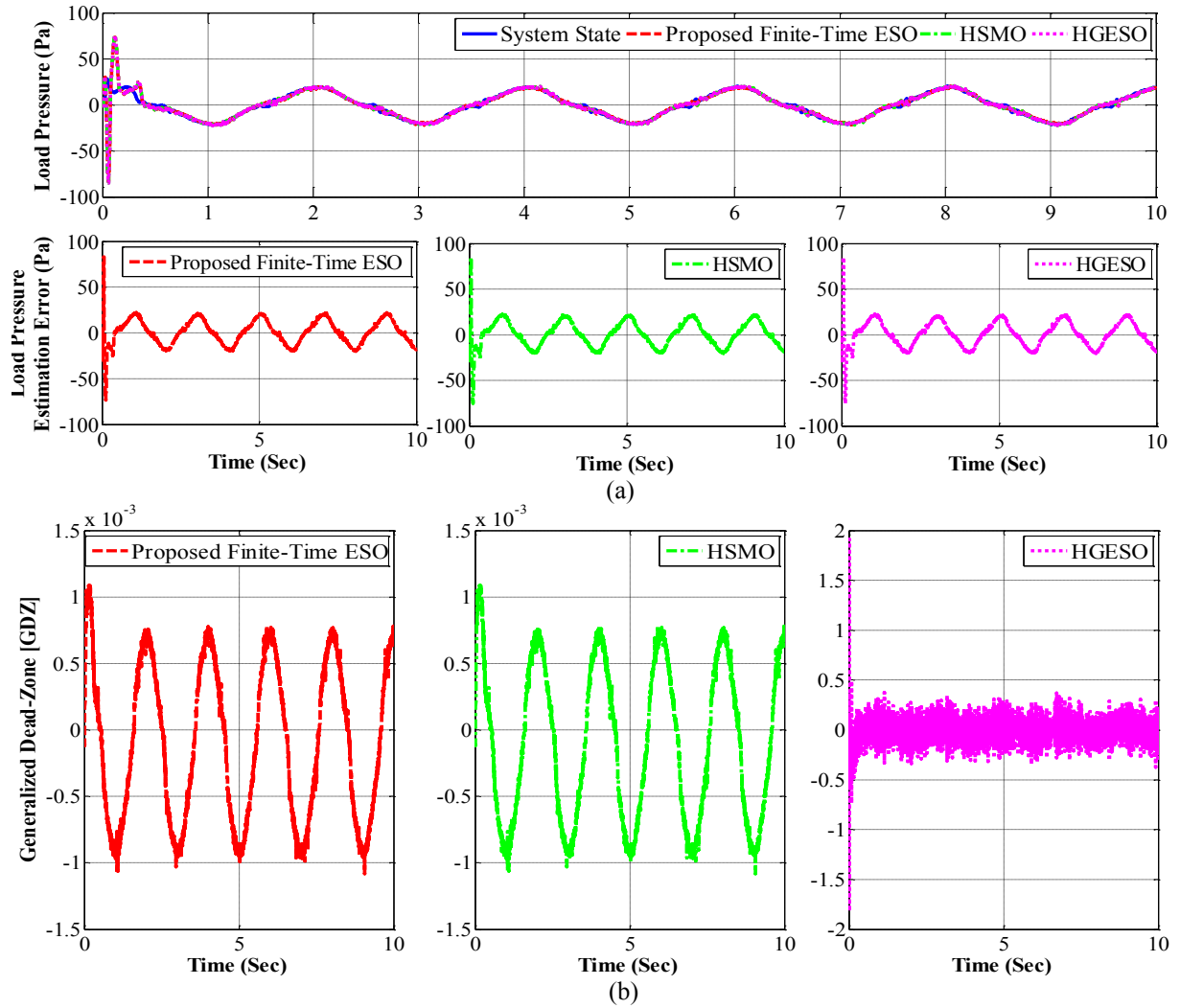


Fig. 10. Real states and estimation results of the second subsystem (Experimental results).

The similarity between the estimation curves in Figs. 9-11 confirms beyond doubt that the proposed scheme is capable to compete with existing

approaches to estimate the full state of the nonlinear system as well as the uncertainties. The proposed observer shows better performance compared to

HSMO for the estimation of the piston velocity and in particular for the spool bias. By comparing experimental results with the simulated ones (Figs. 2-4), it is clear that the performance of the proposed observer is preserved in experiments. For instance, Fig. 9 shows

that the performance of the proposed observer is appropriate in terms of convergence time and estimation errors. Also, its performance for estimating the uncertainties in the experiments is confirmed.

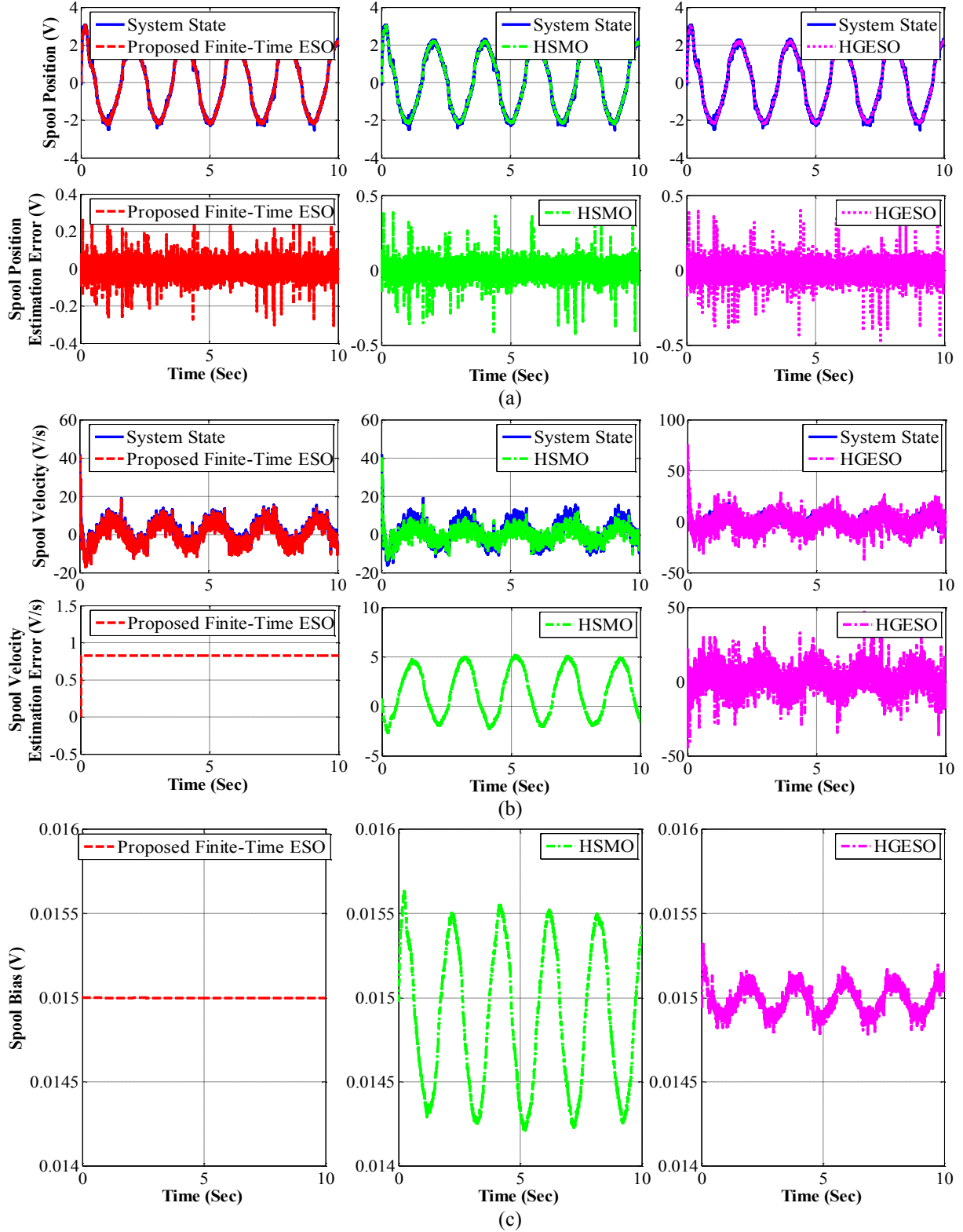


Fig. 11. Real states and estimation results of the third subsystem (Experimental results).

Despite the similarity of the three curves in Fig. 10, the better performance of the proposed observer compared to the other two methods is clearly shown in Fig. 11, where significant differences between the estimation errors are achieved. Finally, by redefining the RMS performance index J_1 for the experimental results, the performance of observers is evaluated in Table 3. This table reports that, while HSMO has slightly better performance on the piston position estimation, it behaves worse than the other observers in almost all the other cases. The proposed observer RMS error is about one fifth of the HSMO one in case of the first subsystem, and less than one third in case of the third subsystem. However, the performance of all three observers is similar for load pressure estimation.

Table 3

Comparative results between the third-subsystem performance indexes.

Methods	Quantity of performance indexes
Proposed finite-time ESO	$J_1 = \begin{bmatrix} 4.349E-12 \\ 1.354E-7 \\ 783.162 \end{bmatrix}$
HSMO [15]	$J_1 = \begin{bmatrix} 3.437E-14 \\ 5.024E-7 \\ 783.162 \end{bmatrix}$
HGESO [27]	$J_1 = \begin{bmatrix} 7.814E-11 \\ 1.949E-7 \\ 759.238 \end{bmatrix}$

Remark 4. Despite the similarity of Figures 2(a,b,c), 5(a,c), 6(b), 9(c), and 10(a) between the proposed approach and the HSMO method, in Figures 3(a) and 9(a) the convergence rate of the proposed approach is a little slower than that of the HSMO method. Figures 3(b), 4(a,b,c), 5(b), 6(a), 7(a,b,c), 9(b), 10(b), and 11(a,b,c) confirm beyond doubt that the proposed scheme is significantly better than existing approaches in the estimation of the full state of the nonlinear system as well as the uncertainties.

Although this paper does not emphasize the absolute superiority of the

proposed approach compared to other methods, based on the results, we conclude that the proposed scheme can compete with the other leading strategies, making it a qualified alternative approach in the observer design with noteworthy potential. The gains of the proposed observer have been computed based on some ordinary algebraic equations, which can be implemented on usual hardware and will not need powerful processors compared to neural network based approaches [34].

6. Conclusions

This paper presented a novel framework to design a finite-time ESO for a class of uncertain nonlinear systems and the method is validated by considering an EHA as the case study. To make the observation errors uniformly bounded, a novel time-varying and free of chattering ESO is designed. To achieve finite-time convergence, novel conversions are used to transform the observation error dynamic to the new coordinate. This enables us to select the time-varying gains. In this design process, without any knowledge about the upper bounds of the uncertainties, the convergence of the observation errors to a small neighborhood around zero is achieved at a finite time. Finally, to highlight the efficiency of the proposed framework, several comparative simulations and experimental results are reported. In conclusion, all the aims of this paper are achieved. To summarize, the proposed design of a continuous and chattering-free ESO allows estimating the full state of the nonlinear system as well as the uncertainties without any knowledge about the upper bound of uncertainties. Moreover the observation errors converge to a neighborhood of zero, introducing a time-varying conversion, so that, finite-time boundedness properties of the proposed ESO are guaranteed by using the asymptotic stability methods in a

straightforward manner, and computing the time-varying gains with reasonable amplitudes for experimental studies over long-time intervals. For future works, further development of the proposed finite-time ESO will be carried out in order to update the time-varying gains in comparison with various techniques such as adaptive neural networks and terminal sliding mode observers.

References

- [1] Guo Q, Zuo Z, Ding Z. Parametric adaptive control of single-rod electrohydraulic system with block-strict-feedback model. *Automatica* 2020;113:108807. <https://doi.org/10.1016/j.automatica.2020.108807>.
- [2] Wu J, Huang Y, Song Y, Wu D. Integrated design of a novel force tracking electro-hydraulic actuator. *Mechatronics* 2019;62:102247. <https://doi.org/10.1016/j.mechatronics.2019.06.007>.
- [3] Razmjooei H, Shafiei M.H. A novel finite-time disturbance observer-based partial control design: A guidance application. *Journal of Vibration and Control* 2020;26(11-12):1001-1011. <https://doi.org/10.1177/1077546319890951>.
- [4] Razmjooei H, Shafiei M.H, Palli G, Ibeas A. Chattering-free robust finite-time output feedback control scheme for a class of uncertain non-linear systems. *IET Control Theory & Applications* 2020;14(19):3168-3178. <https://doi.org/10.1049/iet-cta.2020.0910>.
- [5] Zhao J, Yang T, Sun X, Dong J, Wang Z, Yang C. Sliding mode control combined with extended state observer for an ankle exoskeleton driven by electrical motor. *Mechatronics* 2021;76:102554. <https://doi.org/10.1016/j.mechatronics.2021.102554>.
- [6] Zhang L, Wei C, Wu R, Cui N. Fixed-time extended state observer based non-singular fast terminal sliding mode control for a VTVL reusable launch vehicle. *Aerospace Science and Technology* 2018;82:70-79. <https://doi.org/10.1016/j.ast.2018.08.028>.
- [7] Razmjooei H, Shafiei M.H. A new approach to design a finite-time extended state observer: Uncertain robotic manipulators application. *International Journal of Robust and Nonlinear Control* 2021;31(4):1288-1302. <https://doi.org/10.1002/rnc.5346>.
- [8] Slotine J.J, Hedrick J.K, Misawa E.A. On sliding observers for nonlinear systems. *Journal of Dynamic Systems, Measurement, and Control* 1987;109(3):245-252. <https://doi.org/10.1115/1.3143852>.
- [9] Davila J, Fridman L, Levant A. Second-order sliding-mode observer for mechanical systems. *IEEE transactions on automatic control* 2005;50(11):1785-1789. <https://doi.org/10.1109/TAC.2005.858636>.
- [10] Du H, Shi J, Chen J, Zhang Z, Feng X. High-gain observer-based integral sliding mode tracking control for heavy vehicle electro-hydraulic servo steering systems. *Mechatronics* 2021;74:102484. <https://doi.org/10.1016/j.mechatronics.2021.102484>.
- [11] Dolgopolk M, Fradkov A.L, Andrievsky B. Observer-based boundary control of the sine-Gordon model energy. *Automatica* 2020;113:108682. <https://doi.org/10.1016/j.automatica.2019.108682>.
- [12] Xu W, Qu S, Zhao L, Zhang H. An improved adaptive sliding mode observer for middle-and high-speed rotor tracking. *IEEE transactions on power electronics* 2020;36(1):1043-53. <https://doi.org/10.1109/TPEL.2020.3000785>.
- [13] Xiong Y, Saif M. Sliding mode observer for nonlinear uncertain systems. *IEEE transactions on automatic control* 2011;46(12):2012-2017. <https://doi.org/10.1109/9.975511>.
- [14] Razmjooei H, Shafiei M.H. Partial finite-time stabilization of perturbed nonlinear systems based on the novel concept of nonsingular terminal sliding mode method. *Journal of Computational and Nonlinear Dynamics* 2020;15(2):021005. <https://doi.org/10.1115/1.4045632>.
- [15] Palli G, Strano S, Terzo M. Sliding-mode observers for state and disturbance estimation in electro-hydraulic systems. *Control Engineering Practice* 2018;74:58-70. <https://doi.org/10.1016/j.conengprac.2018.02.007>.
- [16] Wang B, Shao Y, Yu Y, Dong Q, Yun Z, Xu DG. High-order terminal sliding-mode observer for chattering suppression and finite-time convergence in sensorless SPMSM drives. *IEEE Transactions on Power Electronics* 2021;36(10):11910-11920. <https://doi.org/10.1109/TPEL.2021.3068495>.
- [17] Palli G, Strano S, Terzo M. A novel adaptive-gain technique for high-order sliding-mode observers with application to electro-hydraulic systems. *Mechanical Systems and Signal Processing* 2020;144:106875. <https://doi.org/10.1016/j.ymssp.2020.106875>.

- [18] Zhai J, Li Z. Fast-exponential sliding mode control of robotic manipulator with super-twisting method. *IEEE Transactions on Circuits and Systems II: Express Briefs* 2021; <https://doi.org/10.1109/TCSII.2021.3081147>.
- [19] Barambones O, Cortajarena J.A, Calvo I, de Durana J.M, Alkorta P, Karami-Mollaei A. Real time observer and control scheme for a wind turbine system based on a high order sliding modes. *Journal of the Franklin Institute* 2021;358(11):5795-5819. <https://doi.org/10.1016/j.jfranklin.2021.05.022>.
- [20] Fridman L, Shtessel Y.B, Edwards C, Yan X.G. Higher-order sliding-mode observer for state estimation and input reconstruction in nonlinear systems. *International Journal of Robust and Nonlinear Control: IFAC-Affiliated Journal* 2008;18(4-5):399-412. <https://doi.org/10.1002/rnc.1198>.
- [21] Levant A. Higher-order sliding modes, differentiation and output-feedback control. *International journal of Control* 2003;76(9-10):924-941. <https://doi.org/10.1080/0020717031000099029>.
- [22] Andrieu V, Praly L, Astolfi A. Homogeneous approximation, recursive observer design, and output feedback. *SIAM Journal on Control and Optimization* 2008;47(4):1814-1850. <https://doi.org/10.1137/060675861>.
- [23] Lopez-Ramirez F, Polyakov A, Efimov D, Perruquetti W. Finite-time and fixed-time observer design: Implicit Lyapunov function approach. *Automatica* 2018;87:52-60. <https://doi.org/10.1016/j.automatica.2017.09.007>.
- [24] Basin M.V, Yu P, Shtessel Y.B. Hypersonic missile adaptive sliding mode control using finite-and fixed-time observers. *IEEE Transactions on Industrial Electronics* 2017;65(1):930-941. <https://doi.org/10.1109/TIE.2017.2701776>.
- [25] Ménard T, Moulay E, Perruquetti W. Fixed-time observer with simple gains for uncertain systems. *Automatica* 2017;81:438-446. <https://doi.org/10.1016/j.automatica.2017.04.009>.
- [26] Wang L, Gao Z, Zhou X, Han Z. Exponential stabilization of a star-shaped thermo-elastic network system based on the extended state observer with time-varying gains, *IEEE Transactions on Automatic Control* 2020;66(1):267-274. <https://doi.org/10.1109/TAC.2020.2976317>.
- [27] Won D, Kim W, Tomizuka M. Nonlinear control with high-gain extended state observer for position tracking of electro-hydraulic systems. *IEEE/ASME Transactions on mechatronics* 2020;25(6):2610-2621. <https://doi.org/10.1109/TMECH.2020.2985619>.
- [28] Guo Q, Yu T, Jiang D. High-gain observer-based output feedback control of single-rod electro-hydraulic actuator. *IET Control Theory & Applications* 2015;9(16):2395-2404. <https://doi.org/10.1049/iet-cta.2014.1158>.
- [29] Holloway J, Krstic M. Prescribed-time output feedback for linear systems in controllable canonical form. *Automatica* 2019;107:77-85. <https://doi.org/10.1016/j.automatica.2019.05.027>.
- [30] Razmjooei H, Shafiei M.H, Abdi E. A novel continuous finite-time extended state observer design for a class of uncertain nonlinear systems. *IEEE Access* 2020. <https://doi.org/10.1109/ACCESS.2020.3043725>.
- [31] Amato F, Ariola M, Dorato P. Finite-time control of linear systems subject to parametric uncertainties and disturbances. *Automatica* 2001;37(9):1459-1463. [https://doi.org/10.1016/S0005-1098\(01\)00087-5](https://doi.org/10.1016/S0005-1098(01)00087-5).
- [32] Khalil H.K, Grizzle J.W. *Nonlinear systems*, Upper Saddle River, NJ: Prentice hall; 2002.
- [33] Hou M, Duan G, Guo M. New versions of Barbalat's lemma with applications. *Journal of Control Theory and Applications* 2010;8(4):545-547. <https://doi.org/10.1007/s11768-010-8178-z>.
- [34] Guo Q, Zhang Y, Celler B.G, Su S.W. Neural adaptive backstepping control of a robotic manipulator with prescribed performance constraint. *IEEE transactions on neural networks and learning systems* 2018;30(12):3572-3583. <https://doi.org/10.1109/TNNLS.2018.2854699>.